



UNIVERSITY OF LEEDS

This is a repository copy of *Reporting the sensitivity of laser-induced fluorescence instruments used for HO₂ detection to an interference from RO₂ radicals and introducing a novel approach that enables HO₂ and certain RO₂ types to be selectively measured.*

White Rose Research Online URL for this paper:
<http://eprints.whiterose.ac.uk/87628/>

Version: Accepted Version

Article:

Whalley, LK, Blitz, MA, Desservettaz, M et al. (2 more authors) (2013) Reporting the sensitivity of laser-induced fluorescence instruments used for HO₂ detection to an interference from RO₂ radicals and introducing a novel approach that enables HO₂ and certain RO₂ types to be selectively measured. *Atmospheric Measurement Techniques*, 6 (12). 3425 - 3440. ISSN 1867-1381

<https://doi.org/10.5194/amt-6-3425-2013>

Reuse

Unless indicated otherwise, fulltext items are protected by copyright with all rights reserved. The copyright exception in section 29 of the Copyright, Designs and Patents Act 1988 allows the making of a single copy solely for the purpose of non-commercial research or private study within the limits of fair dealing. The publisher or other rights-holder may allow further reproduction and re-use of this version - refer to the White Rose Research Online record for this item. Where records identify the publisher as the copyright holder, users can verify any specific terms of use on the publisher's website.

Takedown

If you consider content in White Rose Research Online to be in breach of UK law, please notify us by emailing eprints@whiterose.ac.uk including the URL of the record and the reason for the withdrawal request.



eprints@whiterose.ac.uk
<https://eprints.whiterose.ac.uk/>

1 **Reporting the sensitivity of Laser Induced Fluorescence**
2 **instruments used for HO₂ detection to an interference from**
3 **RO₂ radicals and introducing a novel approach that**
4 **enables HO₂ and certain RO₂ types to be selectively**
5 **measured**

6
7 **L. K. Whalley^{1,2}, M. A. Blitz^{1,2}, M. Desservettaz¹, P.W. Seakins^{1,2} & D. E. Heard^{1,2}**

8 [1] School of Chemistry, University of Leeds, Leeds, LS2 9JT, UK

9 [2] National Centre for Atmospheric Science, University of Leeds, Leeds, LS2 9JT, UK

10
11 **Abstract**

12 Laboratory studies have revealed that alkene-derived RO₂ and longer-chain alkane-derived
13 RO₂ (>C₃) radicals rapidly convert to HO₂ and then to OH in the presence of NO in a
14 Fluorescence Assay by Gas Expansion (FAGE) detection cell (Fuchs et al., 2011). Three
15 different FAGE cells that have been used to make ambient measurements of OH and HO₂ in
16 the University of Leeds ground-based instrument have been assessed to determine the
17 sensitivity of each cell, when operating in HO₂ detection mode, to RO₂ radicals. The
18 sensitivity to this interference was found to be highly dependent on cell design and operating
19 parameters. Under the operating conditions employed during fieldwork undertaken in the
20 Borneo rainforest in 2008, an OH yield of 17% was experimentally determined for both
21 ethene- and isoprene-derived RO₂ radicals. The high pumping capacity of this system,
22 resulting in a short residence time in the cell, coupled with poor mixing of NO into the
23 ambient air-stream for the titration of HO₂ to OH effectively minimised this potential
24 interference. An OH yield of 46% was observed for ethene-derived RO₂ radicals when a
25 smaller detection cell was used, in which the mixing of NO into the ambient air was
26 improved and the cell residence times were much longer. For a newly developed RO_xLIF
27 cell, used for detection of HO₂ and RO₂ radicals, when running in HO₂ mode an OH yield of
28 95% was observed for ethene-derived RO₂ radicals.

1 In experiments in which conditions ensured the conversion of RO₂ to OH was complete, the
2 yields of OH from a range of different RO₂ species agreed well with model predictions based
3 on the Master Chemical Mechanism version 3.2. For ethene and isoprene derived RO₂
4 species, the relative sensitivity of FAGE was found to be close to that for HO₂, with an OH
5 yield of 100% and 92% respectively. For the longer-chain or cyclic-alkane-derived RO₂
6 radicals (> C₃), model predicted OH yields were highly dependent upon temperature. A
7 model predicted OH yield of 74% at 298 K and 36% at 255 K were calculated for
8 cyclohexane derived RO₂ radicals, and an experimental yield of 38% was observed indicating
9 that the temperature within the cell was below ambient owing to the supersonic expansion of
10 the airstream in the low pressure cell.

11 These findings suggest that observations of HO₂ by some LIF instruments worldwide may be
12 higher than the true value if the instruments were sensitive to these RO₂ species. If this is the
13 case, it becomes necessary to compare atmospheric chemistry model simulations to HO₂*
14 observations, where $HO_2^* = [HO_2] + \sum_i \alpha_i [RO_{2i}]$ and α_i is the mean fractional contribution of
15 the RO₂ species that interferes (RO_{2i}). This methodology, however, relies on model
16 simulations of speciated RO₂ radicals, as instrumentation to make speciated RO₂
17 measurements does not currently exist. Here we present an approach that enables the
18 concentration of HO₂ and RO_{2i} to be selectively determined by varying the concentration of
19 NO injected into a FAGE cell. Measurements of [HO₂] and [RO_{2i}] taken in London are
20 presented.

21 **1 Introduction**

22 OH and HO₂ radicals, collectively termed HO_x, together with RO₂ radicals, control the
23 oxidative chemistry in the atmosphere, being responsible for the transformation of primary
24 emissions into secondary pollutants such as NO₂, O₃ and particulates. OH radicals control the
25 lifetime of some greenhouse gases (e.g. CH₄), the production of acidic species (e.g. H₂SO₄)
26 and aerosol precursors such as oxygenated volatile organic compounds. Understanding the
27 behaviour of free-radicals in the atmosphere is of paramount importance in understanding the
28 lifetimes of pollutants and hence the spatial scales of their transport. Predictive models for
29 future air quality and climate change contain complex chemical schemes, and comparison
30 with measurements of free-radicals (the concentrations of which are controlled only by local
31 chemistry and not by transport) in the present atmosphere constitutes one of the best
32 validations of these schemes (Heard and Pilling, 2003). OH and HO₂ radicals in the

1 troposphere have been measured since the early 1990s using laser induced fluorescence (LIF)
2 spectroscopy at low pressure (Fluorescence Assay by Gas Expansion, or the FAGE
3 technique) originally developed by Hard et al. (1979), (1984). The technique employs 308 nm
4 radiation, produced using a variety of laser technologies, to excite OH radicals, which
5 fluoresce; this emission (also at 308 nm) is detected and used to quantify OH. It is also
6 possible to simultaneously detect HO₂ in a second fluorescence cell, by chemical conversion
7 to OH through reaction with NO and subsequent detection by LIF. The technique has been
8 employed by several groups worldwide for the detection of OH and HO₂ (Hofzumahaus et al.,
9 1996; Mather et al., 1997; Kanaya et al., 1999; Creasey et al., 2001; Faloona et al., 2001;
10 Hanisco et al., 2002; Holland et al., 2003; Heard and Pilling, 2003; Stone et al., 2012).
11 Specific to this work, the Leeds ground-based FAGE instrument has been operational since
12 1996 and has detected OH and HO₂ under a variety of conditions ranging from urban (Heard
13 et al., 2004) to clean marine (Whalley et al., 2010). Although the FAGE technique represents
14 an extremely sensitive (typical OH detection limits are in the low to mid 10⁵ molecule cm⁻³)
15 (Heard and Pilling, 2003) and selective method for OH and HO₂ detection, ambient HO_x
16 concentrations are themselves extremely low (OH concentrations are typically a few 10⁶
17 molecule cm⁻³) (Stone et al., 2012), thus, care needs to be taken to ensure that any
18 measurement is not biased by any chemical or spectral interference.

19 A well-documented example of an OH interference comes from the earliest tropospheric LIF
20 instruments (Davis et al., 1981; Ortgies et al., 1980; Shirinzadeh et al., 1987), which used off-
21 resonant pulsed laser excitation of the OH radical at 282 nm, via the
22 A²Σ⁺(v'=1)←X²Π₁(v''=0) transition. These instruments were found to suffer from a
23 considerable interference from laser-generated OH formed by the laser photolysis of ambient
24 ozone and subsequent reaction of O(¹D) with ambient water vapour:



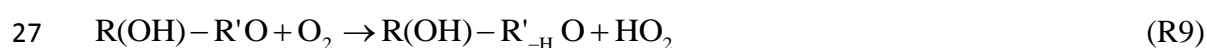
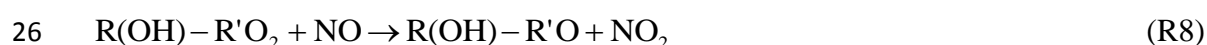
27 The use of OH detection at lower pressure (reducing [H₂O] and hence the rate of R2), lower
28 laser energy per pulse (the OH artefact signal depends on the square of the laser energy) and
29 switching to excitation at 308 nm (the H₂O/O₃ interference is 30 times lower than at 282 nm)
30 almost completely overcame this problem. Holland et al. (2003), however, observed an

1 interference in the presence of ozone and water vapour that appeared to be a dark reaction on
2 the walls of their detection cell which produced a source of HO₂ radicals; the authors report a
3 signal equivalent to 5.4×10⁷ molecule cm⁻³ of HO₂ in the presence of 50 ppbv O₃ and at a
4 relative humidity of 60%. This interference has been characterised in detail and is subtracted
5 from their ambient HO₂ measurements.

6 In the presence of the added NO used to convert HO₂ to OH inside the fluorescence cell, and
7 hence enable HO₂ to be measured, organic peroxy radicals (RO₂) also have the potential to be
8 chemically converted to OH also via:



12 Due to the low pressure employed in FAGE detection, however, R4 is slow (~12 s⁻¹ for CH₃O
13 at 1 Torr) and, given the very short residence time in FAGE between NO injection and the
14 detection region of typically just a few milliseconds or less (Creasey et al., 1997b), it was
15 assumed, until recently, that RO₂ radicals were not converted to OH to any large extent. In
16 support of this, Ren et al. (2004) reported no interference upon introduction of C₁ – C₄ alkane
17 derived RO₂ radicals in the Penn. State FAGE system, and concluded that there was no
18 evidence of any significant interferences for OH or HO₂ measurements in the atmosphere,
19 including in highly polluted urban environments. Only recently has an interference from
20 alkene and aromatic derived RO₂ species been reported (Fuchs et al., 2011). Unlike alkane-
21 derived RO₂ species which are formed via H-atom abstraction from the parent alkane and
22 subsequent addition of O₂ (R6), the major pathway to alkene-derived RO₂ formation is via
23 OH addition across the double bond followed by O₂ addition (R7):





3 The β -hydroxyalkylperoxy radical formed reacts with NO to form the β -hydroxyalkoxy
4 radical (R8) which can either react with O_2 (R9) or decompose to a hydroxyalkyl radical
5 (R10) which then reacts rapidly with O_2 to form a carbonyl and HO_2 (R11). Compared to the
6 slow $RO + O_2$ reaction ($k = 1.65 \times 10^{-15} \text{ cm}^3 \text{ molecule}^{-1} \text{ s}^{-1}$, for $R = CH_3$, R9 (Orlando et al.,
7 2003)), decomposition and subsequent reaction of the hydroxyalkyl radical (CH_2OH) with O_2
8 is fast ($k = 9.6 \times 10^{-12} \text{ cm}^3 \text{ molecule}^{-1} \text{ s}^{-1}$ (Atkinson et al., 1997)). Fuchs et al. (2011) found,
9 due to this rapid decomposition pathway, that RO_2 species formed from alkene and aromatic
10 precursors were detected as OH with relative sensitivities greater than 80% with respect to
11 that for detection of HO_2 in their FAGE system. The level of the interference was found to be
12 highly dependent upon the NO concentration injected and reaction time between injection
13 and OH detection, which was varied by Fuchs et al., suggesting that other FAGE instruments
14 with different cell designs and operational parameters may display different sensitivities
15 towards this interference. FAGE cells used for airborne HO_2 measurements tend to have
16 longer inlets to extend through the fuselage of the aircraft and, hence, sampled air tends to
17 have longer residence times in these cell types compared to cells used solely for ground
18 measurements. Very recently, Mao et al. (2012) reported an average RO_2 sensitivity of ~60%
19 with respect to that for HO_2 for a selection of alkene-derived RO_2 species in the Penn. State
20 FAGE instrument, whilst Vaughan et al. (2012) reported a sensitivity to ethene-derived RO_2
21 radicals of 40% with respect to that for HO_2 for the University of Leeds aircraft FAGE
22 instrument (Commane et al., 2010). Ultimately, the measurement bias on the HO_2
23 concentrations reported from past field studies will depend upon the individual FAGE
24 instruments utilised (because of variations in key operating parameters such as residence
25 time) and the concentration and speciation of RO_2 present. Many FAGE groups now report
26 HO_2^* for comparison with atmospheric chemistry box models (Lu et al., 2012) where HO_2^*
27 $= [HO_2] + \sum_i \alpha_i [RO_{2i}]$, and α_i is the mean fractional contribution of the RO_2 species that
28 interfere (RO_{2i}) in a particular instrument which has been determined experimentally.

29 Together with an HO_2 interference, FAGE measurements of OH are reported to have an
30 interference for one instrument type in forested environments (Mao et al., 2012). The authors
31 postulate that OH may be generated in their FAGE cell in the presence of ozone and alkenes,

1 with laser-generated OH within the cell being ruled out. Similar to the HO₂ interference
2 reported here, this OH interference may be dependent upon the particular design of this
3 FAGE cell, for example the residence time between sampling and detection and, as such, the
4 extent that other OH measurements suffer from this interference is unknown, meaning that it
5 is critical that a set of standardised experiments are performed on different FAGE cell types
6 used for ambient detection of OH to assess the extent of any interference. Good agreement
7 between two independent OH measurements made using Differential Optical Absorption
8 Spectroscopy (DOAS) and LIF was observed during a series of experiments performed in the
9 SAPHIR atmospheric simulation chamber under a range of atmospheric conditions (Fuchs et
10 al., 2012;Fuchs et al., 2013) suggesting that the Julich FAGE system, at least, does not suffer
11 an interference when detecting OH under the conditions studied.

12

13 In this paper we report results from interference studies performed using the University of
14 Leeds ground-based FAGE instrument (Creasey et al., 1997a, Whalley et al., 2010)
15 measuring in HO₂ mode (NO added to the detection cell) and discuss the likely impact of the
16 RO₂ interference on previous field studies. We also compare absolute yields of OH from
17 alkene-derived and higher alkane-derived RO₂ species in the presence of NO with MCMv3.2
18 recommendations, where experimental conditions allowed reactions to proceed to
19 completion. .

20 **2 Experimental**

21 HO₂ and RO₂ radicals were generated prior to FAGE detection by two different methods: a
22 steady-state turbulent flow tube reactor calibrated for absolute radical concentrations and a
23 time-resolved laser flash photolysis system. Each method will be described in turn.

24 **2.1 Steady state experiments**

25 The FAGE calibration system (described in detail by Commane et al. (2010)) acts as a
26 turbulent flow reactor and generates known and equal quantities of OH and HO₂ radicals by
27 the 184.9 nm photolysis of H₂O vapour by a Hg penray lamp in a humidified air stream (R12
28 – 13):

29



1
2 With knowledge of the product of the lamp flux and irradiation exposure time past the lamp
3 (determined by N₂O actinometry (Commane et al., 2010)) the concentration of OH and HO₂
4 may be determined; typical radical concentrations generated by this method range from <10⁷
5 – 10⁹ molecule cm⁻³. RO₂ radicals (in the presence of HO₂ from R13) were generated by
6 introducing the parent hydrocarbon into the FAGE calibration system approximately 2.5 cm
7 after the penray lamp. The OH generated in the calibration photolysis region reacted rapidly
8 with the hydrocarbon introduced, (R6), generating RO₂ radicals. To assess the magnitude of
9 any HO₂ interference suffered during previous ambient field measurements, a number of
10 individual peroxy radical species were generated and introduced into three different
11 fluorescence cells (Fig. 1) which have been used during field deployments by the Leeds
12 group (further details on the fieldwork FAGE detection cells tested are given in section 2.1.1
13 below). The peroxy radicals tested were derived from methane, propane, ethene, isoprene,
14 toluene, cyclohexane and methanol. A small flow (~10 - 150 Standard Cubic Centimetre per
15 Minute, SCCM) of a dilute (0.1 – 5%) hydrocarbon mix in N₂ (ethene, isoprene, toluene,
16 cyclohexane or methanol) or a 100% hydrocarbon flow of propane (10 SCCM) or methane
17 (500 SCCM) was introduced into a 20 – 40 Standard Litre per Minute (SLM) humidified air-
18 stream approximately 5 cm before the exit of the calibration tube. The residence time within
19 the calibration flow tube (~ 10 ms at 40 SLM) was sufficient to ensure complete conversion
20 of OH to RO₂ before being sampled in the fluorescence cells. In the case of ethene, at an
21 initial concentration of 3.1×10¹⁴ molecule cm⁻³, it takes ~1 ms for complete conversion of OH
22 to RO₂, using a rate coefficient, $k_{\text{C}_2\text{H}_4+\text{OH}}$, equal to 2.86×10⁻¹¹ molecule⁻¹cm³s⁻¹ (Cleary et al.,
23 2006). This could be experimentally verified by observing the complete loss of the OH signal
24 upon addition of the hydrocarbons when no NO was added to the FAGE expansion cells; this
25 complete loss of OH signal was observed even for the slowest reacting hydrocarbon species,
26 methane.

27

28 **2.1.1 FAGE detection cells**

29 The University of Leeds ground-based FAGE instrument described in detail elsewhere
30 (Whalley et al., 2010) was assessed to determine the magnitude of the HO₂ interference from
31 selected RO₂ species under configurations employed in two recent field studies. The first, the
32 Oxidants and Particle Photochemical Processes (OP3) (Hewitt et al., 2010) which took place

1 in the Borneo rainforest (Whalley et al., 2011) and the second, the Hill Cap Cloud Thuringer
2 – 2010 (HCCT-2010) (Whalley et al., 2013) which aimed to quantify the loss of radicals to
3 cloud droplets.

4 The operational parameters of the different FAGE fluorescence cells considered are quite
5 different and are summarised in Table 1. During OP3, one 22 cm internal diameter
6 cylindrical, stainless steel fluorescence cell (cell A) was used to make sequential
7 measurements of OH and HO₂ (Fig. 1a). Air was drawn into the cell via a 5 cm tall, 2.54 cm
8 diameter turret through a 1 mm diameter pinhole nozzle in a flat plate (0.1 mm thickness).
9 The cell was maintained at approximately 0.9 Torr using a Roots blower backed by a rotary
10 pump (Leybold). The cell was connected to the pump system via a 10 cm ID, 5 m length
11 stainless steel flexible hose. NO was injected into the cell 7.5 cm below the nozzle via a
12 custom-built injection ring containing four injection points, spaced 4 cm apart, and made
13 from 1.6 mm (ID) tubing in a square arrangement located around the air stream. 50 SCCM
14 NO was injected into the cell via a computer-controlled solenoid valve (Metron
15 Semiconductors) and calibrated mass flow controller (MKS 1179A, range 0 – 50 SCCM)
16 during the second half of the collection period when the laser was tuned to the OH transition.
17 As only one cell was used for sequential detection of OH and HO₂, the conditions were
18 optimised to maximise the sensitivity towards OH. Under these conditions the conversion of
19 HO₂ to OH was only ~ 10%, most likely due to poor mixing of the NO into the ambient air
20 flow caused by the particular flow characteristics created by the combination of the 1 mm
21 diameter pinhole nozzle and the pressure and pumping speeds employed. The 10%
22 conversion of HO₂ to OH determined assumes that there is no preferential loss of either
23 radical in the calibration system, i.e. that the concentration of OH and HO₂ are equal as they
24 enter the FAGE detection cell. This assumption has previously been verified by addition of
25 sufficient CO to the calibration system so as to rapidly convert all the OH to HO₂ (R16) and
26 the HO₂ signal was observed to double in the presence of CO. The radicals sampled, or
27 converted from HO₂, were electronically excited at 308 nm, approximately 13 cm below the
28 sampling nozzle using a tuneable, 5 KHz pulse repetition frequency laser (Nd:YAG pumped
29 Ti:Sapphire, Photonics Industries) with the fluorescence at the same wavelength detected
30 perpendicular to the laser axis by a filtered (Barr Associates filter, transmission > 50% at 308
31 nm) channel photo-multiplier (CPM, Perkin Elmer) and gated-photon counting.

1 During the HCCT-2010 campaign a single FAGE fluorescence cell was used to measure both
2 radical species (Cell B). The cell was operated from the top of a 22 m high tower to co-locate
3 with hill-cap cloud measurements and ensure that the radical measurements were performed
4 in full cloud when it had formed. As a result of these requirements a smaller cell, based on
5 the University of Leeds aircraft FAGE fluorescence cell (Commane et al., 2010), was used to
6 make sequential measurements of OH and HO₂ (Fig. 1b); operational details are provided in
7 Table 1. NO (10 SCCM) was injected into this cell via 3.2 mm ID stainless tubing inserted
8 into the centre of the ambient air stream. This configuration resulted in a high conversion of
9 HO₂ to OH (~90%). Ambient air was drawn into the cell through a 1 mm diameter pinhole
10 nozzle into a 4.5 cm (ID) stainless steel cylinder. The cell was held at 1 Torr and was
11 connected to the roots-rotary pump system described above via 30 m of flexible hosing (5 cm
12 ID). Laser light was delivered from the Nd:YAG pumped Ti:Sapphire laser system to the cell
13 via a 30 m fibre optic. The distance between sampling nozzle and detection was 18 cm with
14 the NO injected ~8 cm below the nozzle.

15

16 The third FAGE cell (Cell C) tested for an RO₂ interference was a recently developed
17 fluorescence cell designed for the detection of RO₂ radicals, alongside OH and HO₂, using
18 the 'RO_xLIF' methodology outlined by Fuchs et al. (2008). The RO₂ cell is operated in two
19 modes, providing a measurement of the sum of OH+HO₂ in HO_x mode and the sum of
20 OH+HO₂+RO₂ in RO_x mode. Experiments were run on this third FAGE cell to determine the
21 magnitude of the HO₂ interference suffered from a variety of RO₂ species in the HO_x mode.

22 A similar FAGE fluorescence cell as the one described above (Fig. 1a, cell A) was modified
23 by coupling it to a differentially pumped reaction tube (held at approximately 30 Torr) to
24 allow for conversion of RO₂ radicals to OH (Fig. 1c). The reaction tube is an 83 cm high, 6.4
25 cm diameter aluminium tube which has been coated with halocarbon wax to minimise radical
26 wall losses. Ambient air (7.5 SLM) is drawn into the reaction tube through a 1 mm diameter
27 pinhole drilled into a thin (1 mm thickness), flat plate aluminium inlet nozzle. In HO_x mode,
28 250 SCCM of CO (5% in N₂, BOC) is flowed into the centre of the reaction tube just beneath
29 the inlet (~ 2 cm below) via a 6.4 mm (ID) stainless steel tube. Hydroxyl radicals are
30 converted to HO₂ by reaction with CO (R14) as they pass through the reaction tube. Air (~ 5
31 SLM) from the reaction tube is sampled by the FAGE detection cell (held at approximately
32 1.5 Torr) via a 4 mm diameter pinhole nozzle sat on a 5 cm tall turret. Ambient HO₂ (and

1 ambient OH which was converted to HO₂ in the reaction tube) is titrated to OH by NO
2 injected into the cell 7.5 cm below the nozzle and detected by LIF; 100 SCCM of NO was
3 injected into this fluorescence cell to maximise the conversion of HO₂ to OH. In RO_x mode,
4 25 SCCM of a 500 ppmv NO standard in N₂ (BOC) was added to the CO flow to promote
5 conversion of RO₂ to OH (R3 – R5); the excess CO present rapidly converts OH to HO₂
6 (R14) and helps to minimise the overall loss of the radicals to the walls of the reaction tube.
7 Ambient RO₂, HO₂ and OH radicals (converted to HO₂ in the reaction tube) enter the FAGE
8 detection cell, are reconverted to OH by NO and detected as described above.



10 **2.2 Time-resolved experiments using laser flash photolysis**

11 The time-resolved setup was based on a laser-induced pump and probe OH reactivity
12 technique developed by Sadanaga et al. (2004) which uses pulsed 266 nm light to photolyse
13 ozone in a flow tube to generate O(¹D) and, by the subsequent reaction of O(¹D) with H₂O
14 vapour, OH radicals (R1 – 2). The flow tube used here was 173 cm in length with an internal
15 diameter of 5 cm; a schematic of the experimental set-up is shown in Figure 2. The total flow
16 was typically 11 SLM and the pressure in the flow tube was 300 Torr, which was controlled
17 by a valve throttling a rotary pump (Leybold xxx). It should be noted that at the pressures
18 employed in the experiments, the high pressure limit of any pressure-dependent reactions
19 taking place in the flow tube will have been reached and the results presented will be
20 applicable to atmospheric conditions. A FAGE cell was located approximately halfway along
21 the flow tube, held perpendicular to the flow tube, and sampled the gas flow through a 1 mm
22 diameter pinhole nozzle that was located within 1 cm of the central axis of the flow tube. At
23 the flow rates and pressure employed, the residence time in the flow tube before sampling
24 was ~ 4 s. A YAG laser (Spectron SL803) was used to generate ~10 mJ pulse⁻¹ of 266 nm
25 photolysis radiation with a 10 ns pulse width. The laser beam profile was shaped using a
26 Galilean telescope to produce a collimated beam with a diameter of ~2 cm and directed along
27 the flow tube such that the outer edge just illuminated the pinhole – gauged by the silhouette
28 of the beam profile at the end of the tube.

29 The FAGE expansion cell was pumped by a rotary / roots blower pump combination
30 (Leybold xxx/yyy), which reduced the pressure in the expansion cell to 1 Torr, and typically
31 sampled about 30% of the total flow of the flow tube with the remaining flow evacuated from

1 the flow tube via the rotary pump. The expansion cell was 4.5 cm in internal diameter with
2 the fluorescence detection axis ~ 23.5 cm from the pinhole. An excimer (Lambda Physik
3 LPX105) pumped dye laser (Lambda Physik FL3002) operating on Rhodamine 6G generated
4 visible light which was frequency doubled to 307.844 nm and used to probe the OH radical
5 via the $Q_1(1)$ (A-X) (0-0) transition; typical pulse energies and pulse lengths were 0.2 mJ
6 pulse⁻¹ and 20 ns respectively. The radiation was directed into the detection axis via a baffled
7 entrance arm and the fluorescence was captured by a filtered (Barr Associates), gated CPM
8 (Perkin Elmer) mounted at right-angles to the laser beam. The pump and probe lasers were
9 typically operated with a pulse repetition frequency of 2.5 Hz.

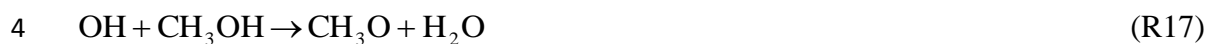
10 A LabViewTM program controlled the experiment via a GPIB interfaced to a delay generator
11 (Berkley Nucleonics Corporation, BNC 555) and an oscilloscope (LeCroy LT264). The time
12 between the photolysis and probe lasers was controlled by the delay generator, and OH time
13 profiles were built-up by scanning the delay between the lasers over 200 points. At each time
14 point the OH fluorescence signal was integrated across its entire decay on the oscilloscope
15 before being transferred for storage on the computer.

16 Gases were introduced to the flow tube via calibrated mass flow controllers (MKS). Nitrogen
17 (10 SLM), was passed through a water bubbler (HPLC grade) and then into a manifold to mix
18 with oxygen (1 SLM), ozone (≤ 10 standard cubic centimetres - SCCM) and a reagent gas (\leq
19 40 SCCM), before admission into the flow tube. Although the O₂ mixing ratio of the total
20 flow was only ~ 0.1 , this was sufficient to drive completely RO₂ formation in the flow tube
21 (and OH formation within the FAGE cell in the presence of NO), and so behaves in the same
22 way as an O₂ fraction of 0.2. Ozone from an ozone generator (Easelec, ELO-3G) was used
23 directly to fill a 5 L Pyrex bulb, and then pressurized with nitrogen (up to 2 bar) to give
24 concentrations between 1 – 3%. The reagent gases, methanol, n-butane, n-pentane, ethene,
25 isoprene and cyclohexane were degassed by freeze pump thawing, and known concentrations
26 were prepared in Pyrex 5 L bulbs. Pressure gauges (MKS) were used to determine the bulb
27 concentrations and the pressure in the flow tube and FAGE cell.

28 The OH generated (approximately 10^{10} molecule cm⁻³) via the photolysis of ozone in the
29 presence of H₂O vapour (R1 – 2) reacted rapidly with the added reagents (at a rate of >1000
30 s⁻¹) in the presence of O₂ forming peroxy radicals (R6) or in the case of methanol, HO₂
31 formed via the following reactions:



3 or



6 OH reacts with methanol, predominantly forming CH₂OH (reported yields of 0.75 – 0.85
7 (Atkinson et al., 2004)) (R15) which then rapidly reacts with O₂ ($9.6 \times 10^{-12} \text{ cm}^3 \text{ molecule}^{-1} \text{ s}^{-1}$)
8 ¹) (Atkinson et al., 2004) to form HO₂ (R16). The other, minor, abstraction channel produces
9 CH₃O, which reacts slower with O₂ ($1.92 \times 10^{-15} \text{ cm}^3 \text{ molecule}^{-1} \text{ s}^{-1}$) (Atkinson et al., 2004)
10 to produce HO₂ (R17, 18). HO₂ generated in the system was detected by adding nitric oxide
11 (NO – 99.95%, BOC) to the FAGE expansion cell (Fig. 2) to titrate to OH for subsequent
12 detection (R5). The NO flow, controlled by a mass flow controller (Brookes) (0 – 50 SCCM),
13 was injected into the centre of the FAGE cell, via 3.2 mm stainless steel tubing,
14 approximately 13.75 cm below the pinhole. The fluorescence signal observed when NO was
15 added to the expansion cell derived from OH and converted HO₂ (OH + αHO₂), where α is
16 equal to the titration efficiency of reaction R5, which is a function of the amount of NO
17 added and the contact time in the expansion cell. For complete conversion of HO₂ to OH in
18 the detection cell α will equal 1. If this is the case, in the presence and absence of methanol
19 there should be no overall change in the initial fluorescence signal when NO was added as the
20 OH lost in reaction R15 is rapidly converted to HO₂ in reaction R16 and then back to OH via
21 reaction with NO. In the time-resolved experiments, a 6 SCCM flow of NO was found to
22 provide the maximum conversion of HO₂ to OH (close to 100%).

23 **2.3 Model comparison**

24 The measured HO₂ yields from the different RO₂ species studied have been compared with
25 model predictions based on the Master Chemical Mechanism (MCM) version 3.2
26 (<http://mcm.leeds.ac.uk/MCM/home.htm>) (Jenkin et al., 1997; Carslaw et al., 1999b; Saunders
27 et al., 2003; Jenkin et al., 2003; Bloss et al., 2005). The chemical reactions which convert the
28 various VOC tested to OH that were incorporated in the model are listed explicitly in the
29 Supplementary Information (SI). The MCM makes the assumption that alkoxy radicals either

1 react with O₂ to form a carbonyl species and HO₂ or decompose (or in the case of the >C₃
2 alkane-derived alkoxy radicals, isomerise) to form a hydroxyalkyl radical. Within a low
3 temperature FAGE expansion, however, in the presence of NO, the reaction of alkoxy
4 radicals and NO may begin to compete as the rate of decomposition and isomerisation slows
5 considerably at reduced temperatures (as discussed further in Section 4, temperatures may
6 drop as low as 25 K within the jet and remain below ambient temperatures in the region
7 between NO injection and detection (Creasey et al., 1997b)). To account for this, (R19) has
8 been included in model predictions with all rate coefficients for the reaction of various RO
9 radicals with NO taken from the review paper by Heicklen (2007).



11 For reactions between alkoxy radicals and NO which do not have reported rate coefficients,
12 $k_{\text{RO}+\text{NO}} = 3.3 \times 10^{-11} \text{ cm}^3 \text{ molecule}^{-1} \text{ s}^{-1}$, (average rate coefficient for reaction of C₃ – C₅ RO
13 radicals with NO) was assumed. The model was initialised with the radical concentrations
14 used and [NO] and [O₂] which encompassed experimental conditions within the FAGE
15 expansion cell. The concentrations of all other intermediate species or products were
16 initialised as zero. [NO] was varied between $1 \times 10^{13} - 1 \times 10^{15} \text{ molecule cm}^{-3}$ depending
17 upon the NO flow rates introduced to each of the FAGE detection cells. For the large FAGE
18 detection cell (of the style cell A), good agreement between the model and experiment is only
19 achieved if the concentration of NO in the jet is lower than that calculated from the initial NO
20 injection flow rate suggesting that the mixing within the jet is poor for this cell (see section
21 4.2 for further details). The simultaneous rate equations were solved using an Excel based
22 integrator, Kintecus (Ianni, 2002). The model runs were 80 ms in duration, which provided
23 sufficient time for complete conversion of peroxy radicals to OH under the time-resolved
24 experimental conditions discussed above.

25 **3 Results**

26 **3.1 RO₂ interferences in HO₂ measurements using fieldwork FAGE** 27 **instrumentation**

28 A variety of RO₂ species were generated in the turbulent flow reactor and introduced into the
29 three FAGE cells, A-C (Fig. 1) described in section 2.1.1. The yield of OH from the different
30 RO₂ species for the different cells is given in Table 1. The flow reactor produces OH and

1 HO₂ in equal quantities in the absence of a hydrocarbon (Fuchs et al., 2011). Upon addition
2 of a hydrocarbon all the OH generated is quickly consumed (on a timescale of the order of
3 1×10⁻⁴ s) and RO₂ radicals form. In the case of propane or methane, the RO₂ formed does not
4 yield appreciable OH (via the formation of HO₂) in the FAGE expansion cells in the presence
5 of NO (as shown by the time-resolved experiments, section 3.2, the OH yield from propane
6 was <4%), and so any fluorescence signal observed upon NO addition relates solely to the
7 co-generated HO₂. The yield of OH from RO₂i species can be determined by comparing the
8 fluorescence signal observed when a RO₂i species was present (HO_x signal_(reagent)) with the
9 OH yield from HO₂ alone (HO₂ signal in the propane or methane experiments, which have no
10 interference) using Eq. 1:

$$11 \quad \text{Relative OH yield} = \frac{\text{HO}_x \text{ signal}_{(\text{reagent})} - \text{HO}_2 \text{ signal}}{\text{HO}_2 \text{ signal}} \quad (1)$$

12 The flows of hydrocarbons were adjusted so that equivalent OH reactivities (k_{HC+OH}[HC]) for
13 each of the hydrocarbons tested were used to ensure that any other loss of OH in the turbulent
14 flow reactor (e.g. loss to walls) did not bias the relative yields determined.

15 In a number of experiments the NO concentration added to detection cell A was varied and
16 the ratio of the OH signal observed for propane-derived RO₂ radicals relative to ethene-
17 derived RO₂ radicals were compared and are shown in Table 1 and Figure 4. As the NO
18 concentration was reduced the interference from alkene-derived RO₂ radicals decreased. By
19 varying [NO], it becomes possible to discriminate ambient RO₂ radicals from ambient HO₂
20 radicals and this is discussed further in Section 4.2.

21 **3.2 Time-resolved experiments**

22 To determine the absolute yield of OH from different RO₂ radicals in the presence of NO, a
23 range of RO₂ radicals (or HO₂ in the case of methanol) were generated by the addition of
24 different parent hydrocarbons to the flow tube described in Section 2.2 coupled to a FAGE
25 cell in which there was sufficient time for complete conversion of RO₂ to OH. The time-
26 resolved flow tube experiments were not performed on a field instrument used for ambient
27 HO₂ detection and so the purpose of these experiments, rather than gauge the level of
28 interference suffered, was to experimentally determine the yield of OH from a range of RO₂
29 radicals in the presence of NO to compare to MCM recommendations. The time-resolved

1 experiments enabled long reaction times to be reached, allowing the conversion of RO₂ to
2 OH to proceed to completion, and providing a measure of the asymptotic yields of HO₂.

3 The time-resolved OH signals observed for a selection of RO₂ species tested are shown in
4 Figure 3, and Table 2 summarises the OH yields for all RO₂ investigated. In the absence of
5 reagent, an OH signal was observable (upper panel, Fig. 3) which decayed at a rate of ~25 s⁻¹.
6 This loss can be attributed to reaction of OH with ozone that was present and diffusion of the
7 radical out of the photolysis beam area. Upon addition of a reagent to the flow tube, OH was
8 converted to RO₂ at >1000 s⁻¹. This rapid conversion ensured that the different RO₂ generated
9 were present at the same concentration as each other (allowing relative yields to be
10 determined) and that all the OH initially generated was consumed in the flow tube (given the
11 residence time of 4 s) thus allowing a single exponential fit to be applied to the RO₂ signals
12 displayed in the lower panel of Figure 3. The slow decay (~5 s⁻¹) of the radical signal,
13 displayed in the lower panel of Figure 3, may be attributed primarily to diffusion of the
14 radicals out of the photolysis beam area and, to a lesser extent (no greater than 1 s⁻¹), to
15 radical-radical reaction.

16 As the initial OH concentration generated and subsequent HO₂ or RO₂ concentration
17 generated within the flow tube were uncalibrated, the absolute OH yields within the FAGE
18 expansion cell from the different RO₂ species were determined by comparing with the OH
19 signal observed from HO₂ generated in the methanol experiments which has a 100% yield.
20 An exponential function of the form: OHsignal = y₀ + A × exp(-B × probedelay time) was
21 fitted to each OH temporal profile associated with the different RO₂ species investigated. To
22 determine the relative yields of OH, the ratio of the A factor for each fit relative to the A
23 factor determined for the methanol fit was calculated using Eq. 2:

$$24 \quad \text{Relative OH yield} = A \text{ factor}_{(\text{reagent})} : A \text{ factor}_{(\text{methanol})} \quad (2)$$

25 In agreement with Fuchs et al. (2011), a large OH yield from alkene-derived RO₂ radicals
26 was observed (see Table 2) when NO was present in the FAGE cell. Smaller, but still
27 significant, OH yields were also observed for RO₂ radicals derived from cyclohexane, n-
28 butane and n-pentane (Table 2); the OH signal observed for propane-derived RO₂ radicals
29 was negligible (upper limit of 4%).

1 In several experiments, it was found that ethene-derived RO₂ radicals when compared to HO₂
2 from methanol had OH yields greater than one. The formation of β-hydroxy peroxy radicals
3 is fast in the flow tube, and, if complete RO₂ titration to HO₂ and ultimately to OH was
4 occurring in the FAGE cell then the ratio of the OH signals observed in the presence of
5 ethene and methanol would be expected to equal one; a value greater than one suggests
6 incomplete conversion of methanol to HO₂ in the flow tube. It was observed in experiments
7 where the Pyrex bulb containing methanol was left for a full day before use to allow for
8 mixing rather than just a couple of hours, that yields closer to one were obtained indicating
9 that in several of the experiments there may have been insufficient methanol reaching the
10 flow tube owing to extremely slow mixing of the gas bulb. To ensure that the results are not
11 biased by a possible problem with methanol, column 2, Table 2 only includes relative OH
12 yields calculated when the methanol bulb had been left for a day or longer. As this constraint
13 limited the amount of data available, a third column which presents the OH yields referenced
14 with respect to ethene (calculated using Eq. 3) is also provided:

$$15 \text{ Relative OH yield} = A \text{ factor}_{(\text{reagent})} : A \text{ factor}_{(\text{ethene})} \quad (3)$$

16 4 Discussion

17 4.1 Time-resolved experiments. Measured and modelled HO₂ yields following 18 complete conversion of RO₂

19 Under conditions optimised for complete conversion of RO₂ radicals to OH in a FAGE cell
20 with added NO, i.e. very long reaction times, the yield of HO₂ from a number of alkene-
21 derived RO₂ species compares favourably to the MCMv3.2 predictions of the OH yield
22 determined using Eq. 4 after a reaction time of 9.8 ms, as shown in Table 2, suggesting that
23 the yield of HO₂ from other RO₂ species not measured here can be derived with some
24 confidence from MCM predictions for this particular experimental set-up.

$$25 \text{ MCMOH yield} = \frac{\text{modelled [OH] generated}}{\text{model initialised [RO}_2\text{]}} \quad (4)$$

26 For >C₃ alkane-derived RO₂ species, the MCM also predicts a non-zero HO₂ yield. For these
27 species, reaction with NO produces an alkoxy radical which can react with O₂ or isomerise
28 forming a β-hydroxyalkylperoxy radical in the presence of O₂, which for the case of n-butane
29 derived peroxy radical is:



4 The alkoxy radical, C_4H_9O , may also react with NO under FAGE conditions:



6 As shown in reactions (R8 – R11) the β -hydroxyalkylperoxy radical can react further with
7 NO and decompose rapidly in the presence of O_2 to form HO_2 . However, as seen in Table 2,
8 the MCM over-predicts the yield of HO_2 at 298 K from n-pentane and cyclohexane derived
9 peroxy radicals, and under-predicts the OH yield from n-butane-derived alkanes. The
10 modelled to measured agreement for n-pentane and cyclohexane derived RO_2 radicals can be
11 improved if the rate coefficient for isomerisation (R21) is reduced by assuming a lower
12 temperature; it was found by varying the temperature in the model that 255 K provided the
13 best agreement for all RO_2 species considered (Table 2). In the case of cyclohexane, the rate
14 coefficient for isomerisation (taken from the MCMv3.2) decreases from $6.3 \times 10^4 \text{ s}^{-1}$ to $2.1 \times$
15 10^3 s^{-1} as the temperature was reduced from 298 K to 255 K. Stevens et al. (1994) report a
16 temperature of 245 K within the Penn State FAGE instrument as an airstream enters the
17 detection cell and accelerates to velocities of $>300 \text{ ms}^{-1}$; at the laser detection axis the
18 velocity is reduced to $\sim 50 \text{ ms}^{-1}$ and the air temperature increases to ambient levels once more.
19 Similarly, measurements of rotational temperatures and computational fluid dynamic (CFD)
20 calculations performed to determine the temperature and density profiles of an airstream
21 within a Leeds FAGE detection cell, type A (Fig 1a), suggest that air temperatures drop as
22 low as 25 K in the first 2 cm in the detection cell beneath the pinhole as the airstream
23 expands supersonically and reaches velocities of 750 ms^{-1} before slowing and increasing back
24 to ambient temperatures at the detection axis (Creasey et al., 1997b). Taking these
25 temperature profiles into account, it is expected that the mean temperature experienced
26 between pinhole and the detection axis will be below ambient and if this is the case the rate
27 coefficient for isomerisation will slow considerably (Orlando et al., 2003). At lower
28 temperatures the reaction between an alkoxy radical and NO (R19) can begin to compete with
29 the isomerisation reaction (R21) and can, as a result, lower the overall OH yield observed
30 from these RO_2 radicals. This effect reduces the agreement between the experimental and

1 modelled OH yield from n-butane-derived RO₂ further suggesting that the rate coefficient for
2 isomerisation of the C₄H₉O alkoxy radical may actually be faster than assumed in the model.
3 There is very little information on the temperature dependence associated with the rate of β-
4 hydroxyalkoxy decomposition in the literature. A theoretical temperature dependence for the
5 rate of decomposition of ethene-derived β-hydroxyalkoxy radical has been reported (Kukui
6 and Le Bras, 2001):

$$7 \quad k_{\text{decomp.}} = 1.1 \times 10^{13} [\text{s}^{-1}] \cdot e^{\frac{-41.84 [\text{KJ/mole}]}{RT}} \quad (5)$$

8 When this temperature dependence is included in model calculations, assuming a temperature
9 of 255 K, the OH yield predicted is reduced by ~ 10% from calculations assuming a
10 temperature of 298 K (Table 2) as the rate coefficient for decomposition decreases from 5.1
11 × 10⁵ s⁻¹ to 3.0 × 10⁴ s⁻¹. Although likely to be similar to that of the ethene-derived alkoxy
12 radical, no information on the temperature dependence of isoprene-derived alkoxy radical
13 decomposition exists in the literature so the impact on the OH yield at reduced temperatures
14 is not considered here.

15 **4.1.2 Magnitude of the interference for fieldwork instruments**

16 For the three fieldwork FAGE cells tested (Fig. 1) which have different residence times and,
17 hence reaction times for RO₂ conversion to OH, the yield of OH from the alkene-derived RO₂
18 radicals was variable. For cell A, CFD calculations have demonstrated that the air stream is
19 significantly accelerated within the cell (and, in turn, is significantly cooled), owing to the
20 supersonic expansion after the small diameter, 1 mm, pinhole. Similar acceleration and
21 cooling may be assumed for cell B as a 1 mm pinhole was again used. In cell C, air entered
22 the FAGE cell through a 4 mm pinhole and so the same level of acceleration or cooling, as
23 predicted in cell A, is not expected. For cell C, it may be expected that NO should mix
24 reasonably well with the ambient air stream also. The best agreement between the MCM
25 predictions and experimental results occurs if a contact time (and [NO]) of ~0.9 ms (and
26 1×10¹⁴ molecule cm⁻³), ~1.9 ms (and 1×10¹⁴ molecule cm⁻³) and ~ 70 ms (and 9.5×10¹⁴
27 molecule cm⁻³) is assumed for cell A, cell B and cell C (Fig. 1) respectively at a temperature
28 of 255 K for cells A and B and 298 K for cell C. For cell A, a residence time from pinhole to
29 detection region of <1 ms has been calculated using CFD (Creasey et al., 1997b) and
30 compares favourably to the estimated contact time of 0.9 ms (estimated from the time at

1 which the modelled yields best agree with the experimental relative yields, Table 1). As it is
2 difficult to calculate the cell residence absolutely, due to the free-jet expansion that occurs,
3 comparison of the yields with model predictions provides a means to gauge the time spent
4 between the NO injection region and detection region experimentally. Uncertainty in the
5 residence time may arise, however, if the NO injected into the cell does not fully mix with the
6 sampled air stream or if the mean temperature of the airstream is not considered or known.
7 Qualitatively, the extent of the interference suffered is directly proportional to residence time
8 within the jet and inversely proportional to the mean temperature experienced by the jet (Eq.
9 6). At ambient temperatures, increasing the NO concentration will lead to an increase in the
10 interference; at reduced temperatures, however, the impact of NO becomes more complex:
11 Increasing the concentration of NO will increase the rates of reactions R3 and R5 but also
12 increases the rate of reaction R19. For alkoxy radicals which display a strong temperature
13 dependence with respect to isomerisation, as is the case for the alkoxy radical derived from
14 cyclohexane (CHEXO), increasing NO concentrations beyond a certain concentration may
15 actually lead to a reduction in the level of interference observed as R19 begins to compete
16 effectively with R21. Model simulations looking at the yield of OH from cyclohexane-
17 derived RO₂ radicals at 255 K predict that at a residence time of 9.8 ms (time over which
18 time-resolved experiments were run) the yield of OH will increase with increasing [NO] until
19 a NO concentration of 1.2×10^{14} molecule cm⁻³ is reached and then the yield will begin to
20 decrease as [NO] increases further. Note, if the residence time is increased, less NO is
21 required to achieve the maximum yield and vice versa. Under the experimental conditions
22 discussed in this paper the OH yield should have been directly proportional to [NO]:

$$23 \quad \text{Interference} \propto \frac{\text{Residence time} \times [\text{NO}]}{\text{Temperature}} \quad (6)$$

24 Fuchs et al. (2011) observed a large under-prediction of the OH yield from cyclohexane-
25 derived RO₂ radicals in the presence of NO and suggested that the model under-prediction for
26 the yield of OH from this species may reflect a missing ring opening mechanism in the MCM
27 which could promote further HO₂ formation. Fuchs et al.(2011) used MCMv3.1 which did
28 not contain a ring opening mechanism to estimate the expected level of interference in the
29 Julich FAGE system. An additional degradation pathway for CHEXO which includes a ring
30 opening route, is included in MCMv3.2 leading to the yield of HO₂ (and ultimately OH,

1 following further reaction) from cyclohexane-derived RO₂ radicals approximately doubling
2 when switching from MCMv3.1 to MCMv3.2 chemistry.

3 **4.2 Minimising the RO₂ interference further**

4 As highlighted in Table 1, a decrease in the amount of NO injected into cell A reduces the
5 OH yield from ethene-derived RO₂ radicals. Reducing the sensitivity of the instrument to the
6 interference, however, leads to a concomitant reduction in HO₂ sensitivity. As only one NO
7 molecule is required to titrate one HO₂ radical to OH, whilst two or more are required for
8 RO₂ to OH titration, it is possible to begin to discriminate between HO₂ and RO₂ by reducing
9 the amount of NO mixed into the jet as shown in Figure 4. For cell A, at an NO concentration
10 of 1×10^{13} molecule cm⁻³, approximately twenty HO₂ radicals titrate to OH for one RO₂i
11 radical conversion to OH; determined from the ratio 'relative OH yield (propane) : relative
12 OH yield (ethene)' with 'relative OH yield' calculated using Eq. 1. At this NO concentration
13 the 5 minute limit of detection of the instrument for HO₂ will be $\sim 4 \times 10^6$ molecule cm⁻³ and,
14 although higher than detection limits from earlier campaigns (e.g. the HO₂ LOD during the
15 SOAPEX campaign which took place in Cape Grim in Australia was 5.4×10^5 molecule cm⁻³
16 for 2.5 minute integration time) (Creasey et al., 2003), the instrument remains sufficiently
17 sensitive for ambient HO₂ detection with minimal RO₂ interference (~5%). It should be noted
18 that agreement between the MCMv3.2 model and observations can only be achieved if it is
19 assumed that 5.5 times less NO is mixed fully into the air sample within the FAGE cell than
20 is actually injected. Even when a reduced [NO] is assumed, the model predicted HO₂:RO₂
21 ratio vs [NO] is not wholly consistent with the ratio observed experimentally. As displayed in
22 Figure 4, the observed ratio increases slower than the model predicts as [NO] decreases (most
23 apparent at the lowest [NO]) suggesting an enhanced RO₂ → OH conversion relative to HO₂
24 → OH conversion. This observation may indicate that HO₂ is preferentially lost in the cell
25 compared to RO₂ radicals, potentially, by more efficient removal of HO₂ relative to RO₂ by
26 H₂O clusters (Creasey et al., 2001). This finding only serves to further highlight the need to
27 experimentally determine the level of interference for each individual FAGE system and
28 specific experimental conditions.

29 As demonstrated by Figure 4, by varying the amount of NO injected it is possible to switch
30 from conditions where certain RO₂ types are efficiently converted to OH (NO > 5×10^{13}
31 molecule cm⁻³) to conditions where the conversion is poor (NO < 1×10^{13} molecule cm⁻³). With

1 knowledge of the conversion efficiency of RO₂ and HO₂ at different NO concentrations,
2 changing the NO flow during ambient measurements can selectively provide a measurement
3 of the concentration of RO_{2i} and HO₂ by solving simultaneous equations (E7 and E8):

$$4 \text{ HO}_x \text{ signal}_{\text{low[NO]}} = C_{\text{HO}_2, \text{low[NO]}} \times ([\text{HO}_2] + \alpha_{\text{low[NO]}} [\text{RO}_{2i}]) \quad (7)$$

$$5 \text{ HO}_x \text{ signal}_{\text{high[NO]}} = C_{\text{HO}_2, \text{high[NO]}} \times ([\text{HO}_2] + \alpha_{\text{high[NO]}} [\text{RO}_{2i}]) \quad (8)$$

6 where HO_x signal is the fluorescence signal observed in cts s⁻¹ mW⁻¹, C_{HO₂} is the sensitivity
7 of the instrument to HO₂ (determined by calibration) at a particular NO flow in units of cm³
8 molecule⁻¹ ct s⁻¹ mW⁻¹ and α is the mean fractional contribution of RO_{2i} at a selected [NO].

9 During a recent field project, the Clean air for London campaign (ClearfLo), this approach
10 was adopted during ambient measurements. The NO concentration injected into a FAGE cell
11 (cell type A) used during the campaign for sequential measurements of OH and HO₂ was
12 varied between ~1 and 9×10¹³ molecule cm⁻³; a measurement of the total [RO₂] was
13 determined simultaneously using the RO_xLIF cell C operating in RO_x mode. The campaign
14 average diurnal profile of HO₂, alkene/aromatic or long-chain alkane-derived RO₂ and short-
15 chain alkane-derived RO₂ radicals selectively measured is provided in Figure 5. The [HO₂]
16 (red) and [RO_{2i}] (mustard, alkene and aromatic RO₂ species)) have been derived using
17 Equation 7 and 8 (i.e. from HO₂* signal observed when using cell A at high and low NO
18 flows; with the sensitivity to HO₂ and RO_{2i} determined experimentally at the two NO flows
19 used). The C1-C3 alkane-derived [RO₂] (green) was determined from cell C detection of total
20 [RO_x] with the derived [HO₂] and [RO_{2i}] subtracted. In generating Figure 5, it was assumed
21 that all RO_{2i} had the same conversion efficiency (α) as ethene-derived RO₂. This assumption,
22 whilst reasonable for other RO₂ radicals derived from other alkenes or aromatic VOC, may
23 positively bias the [RO_{2i}] and negatively bias [HO₂] calculated if longer-chain alkane-derived
24 RO₂ (≥C₄) which have a lower α were present at significant levels. Preliminary box
25 modelling studies run for the ClearfLo project, which were constrained by the measurements
26 of a wide range of VOCs of various classes, demonstrate that aromatic and alkene RO₂
27 species do dominate RO_{2i}, with ≥C₄ alkane-derived RO₂ species only contributing 7 % to all
28 RO_{2i} identified on average. For this particular environment at least (and likely applicable to
29 many others), determining HO₂ and RO_{2i} by the methodology discussed here may provide
30 reasonable results.

1 An alternative approach to partial speciation of RO₂ radical classes would be to use two
2 FAGE cells in which the RO₂ interference is minimised in the first (e.g. cell A, run at a low
3 [NO]) and maximised in the second (e.g. cell C, HO_x mode, run at a high [NO]).

4 **4.3 Impact on previous field studies**

5 The University of Leeds ground-based FAGE instrument has been operational since 1996 and
6 has taken part in 17 campaigns with HO₂ measurements made during 13, see Table 3 for
7 further details. In some of the earlier campaigns good conversion of HO₂ to OH was achieved
8 as two independent cells were used (Smith et al., 2006), with the conditions of one cell
9 optimised for HO₂ detection, and so a significant portion of interfering RO_{2i}, if present, may
10 also have been titrated to OH, constituting an interference. Many of the previous campaigns
11 took place under relatively clean, unpolluted conditions, for example EASE-96 (Carslaw et
12 al., 1999a), EASE-97 (Creasey et al., 2002; Carslaw et al., 2002), SOAPEX (Creasey et al.,
13 2003; Sommariva et al., 2004), NAMBLEX (Sommariva et al., 2006), CHABLIS (Bloss et
14 al., 2010), RHaMBLe (Whalley et al., 2010) where the concentrations of RO_{2i} are likely low
15 and methyl peroxy radicals, which do not give an interference (Ren et al., 2004), were
16 expected to be the dominant RO₂ species; e.g. during EASE-96 the model predicted that 92%
17 of peroxy radicals present were either HO₂ (53%) or CH₃O₂ (39%) during unpolluted
18 conditions (Carslaw et al., 1999a). Similarly, for the SOS project (Vaughan et al., 2012),
19 which took place in Cape Verde, models predicted that ~90% of peroxy radicals were either
20 HO₂ or CH₃O₂. In general, models run for these campaigns tended to over-predict HO₂
21 despite additional HO₂ loss mechanisms such as reaction with halogen oxides and/or
22 heterogeneous loss to aerosol surfaces in the model description. In contrast, under polluted,
23 urban conditions (e.g. PUMA (Heard et al., 2004), TORCH-1(Emmerson et al., 2007))
24 models either significantly under-predicted HO₂ observations (PUMA) (Emmerson et al.,
25 2005) or were in relatively good agreement (TORCH-1) (Emmerson et al., 2007). If elevated
26 concentrations of alkene-derived, aromatic-derived and higher-alkane derived RO₂ species
27 were present, the true ambient HO₂ concentrations, as opposed to HO₂^{*}, were likely lower
28 than reported. It is possible, although difficult to verify without observations of speciated
29 RO₂, that the conclusions drawn from these observations, for example, that additional HO₂
30 sources in models are required to replicate observations, may be in error.

1 Under the operating conditions employed during the OP3 campaign, the instrument was
2 relatively insensitive to detection of RO₂ species. The experiments presented here reveal a
3 17% yield of OH due to the decomposition of ethene-derived RO₂ in the presence of NO in
4 the FAGE detection cell under OP3 conditions. This provides an upper limit to the HO₂ yield
5 from RO₂ species during OP3 as, under conditions in which the interference signal was
6 maximised (Section 3.2), ethene-derived RO₂ species provided the largest HO₂ yield
7 compared with other RO₂ species. Model simulations (Whalley et al., 2011) suggested that up
8 to 2.1×10^8 molecule cm⁻³ of potentially interfering RO₂ species were present at solar noon
9 during OP3 (with isoprene derived peroxy radicals contributing ~60% to this total), and thus
10 up to 3.5×10^7 molecule cm⁻³ of the HO₂ concentration may be attributed to these species
11 (~10% of the total HO₂ signal observed (Whalley et al., 2011)). Model comparisons with the
12 radical measurements made during the campaign demonstrated a large missing OH source
13 and over-predicted the HO₂ observations. The small positive bias on the HO₂ observations,
14 owing to the small yield of HO₂ from RO₂ species, only serves to reduce the modelled to
15 measured agreement further. For the HCCT-2010 campaign, the potential impact of the
16 interfering RO₂ species is greater (Table 1) owing to the smaller cell (with a longer inlet) and
17 longer residence time employed. The campaign took place in a pine forest, close to the
18 summit of Mount Schmücke in the Thüringer Wald mountain range in East Germany, during
19 September and October 2010. VOC measurements were made downwind of the measurement
20 site. Only low concentrations of isoprene (50 pptv) were detected, however, suggesting that
21 the concentration of RO₂i were also low.

22 **5 Conclusions and further work**

23 Recent studies conducted on a number of different fluorescence cells used in the FAGE
24 instrument at Leeds have demonstrated that alkene- and aromatic-derived RO₂ species can
25 yield appreciable quantities of OH upon addition of NO in FAGE detection cells and,
26 therefore, positively bias HO₂ observations if left uncorrected. Many FAGE groups now
27 report HO₂* for comparison with atmospheric chemistry box models to include any
28 interference from RO₂i. As demonstrated in this study, the magnitude of this interference is
29 critically dependent on the cell design, quantity of NO used in the titration, the residence time
30 and mean temperature of the air stream within the FAGE cell. The interference may be
31 minimised by reducing NO concentrations and/or residence time, and although such a
32 reduction will also reduce the sensitivity of the instrument to HO₂ (albeit to a lesser extent

1 than the reduction in the sensitivity to RO₂ radicals) it will still be possible to detect ambient
2 levels HO₂ using FAGE.

3 In laboratory, laser-flash photolysis experiments, under conditions optimised for complete
4 conversion of RO₂ radicals to OH in a FAGE cell, the yield of HO₂ from a number of alkene-
5 derived RO₂ species could be measured, and compared favourably with MCMv3.2
6 predictions. This suggests that the yield of HO₂ from other alkene-derived or aromatic-
7 derived RO₂ species not tested here, but which are expected to exhibit high yields, could be
8 determined from MCM predictions. The ability to discriminate between HO₂ and RO₂i
9 radicals, as illustrated for the ClearfLo project, is not only of great value for field
10 measurements (and subsequent model comparisons), but such instrumentation may be used to
11 selectively determine the yield of HO₂ in laboratory experiments under conditions where RO₂
12 radicals may also be present. Important applications, for example, would be the experimental
13 verification of a significant prompt HO₂ yield from OH initialised isoprene oxidation, as
14 proposed by Peeters et al. (2009) or prompt HO₂ yields from OH initialised oxidation of
15 aromatics (Nehr et al., 2012).

16 This study demonstrates that some of the previous HO₂ measurements that depend upon
17 chemical titration to OH by NO may suffer an interference due to partial detection of RO₂
18 radicals. Under conditions where there are significant alkene, aromatic or long-chain alkanes
19 present, the HO₂* concentration which was measured will have been higher than the HO₂
20 concentration that was actually present. Models have over-estimated HO₂ concentrations
21 under such conditions, and this over-estimation would only increase if the observations of
22 HO₂ were corrected for the interference suggesting there is a major gap in our understanding
23 of the chemistry controlling these radicals.

24

25 **Acknowledgements**

26 We would like to thank the National Centre for Atmospheric Science (NCAS) for financial
27 support and EUROCHAMP is acknowledged for PWS.

28 **References**

29 Atkinson, R., Baulch, D. L., Cox, R. A., Hampson, R. F., Kerr, J. A., Rossi, M. J., and Troe, J.: Evaluated
30 kinetic, photochemical and heterogeneous data for atmospheric chemistry .5. IUPAC Subcommittee

1 on Gas Kinetic Data Evaluation for Atmospheric Chemistry, *J Phys Chem Ref Data*, 26, 521-1011,
2 1997.

3 Atkinson, R., Baulch, D. L., Cox, R. A., Crowley, J. N., Hampson, R. F., Hynes, R. G., Jenkin, M. E., Rossi,
4 M. J., and Troe, J.: Evaluated kinetic and photochemical data for atmospheric chemistry: Volume I -
5 gas phase reactions of O_x, HO_x, NO_x and SO_x species, *Atmospheric Chemistry and Physics*, 4, 1461-
6 1738, 2004.

7 Bloss, C., Wagner, V., Jenkin, M. E., Volkamer, R., Bloss, W. J., Lee, J. D., Heard, D. E., Wirtz, K.,
8 Martin-Reviejo, M., Rea, G., Wenger, J. C., and Pilling, M. J.: Development of a detailed chemical
9 mechanism (MCMv3.1) for the atmospheric oxidation of aromatic hydrocarbons, *Atmos Chem Phys*,
10 5, 641-664, 2005.

11 Bloss, W. J., Camredon, M., Lee, J. D., Heard, D. E., Plane, J. M. C., Saiz-Lopez, A., Bauguitte, S. J. B.,
12 Salmon, R. A., and Jones, A. E.: Coupling of HO_x, NO_x and halogen chemistry in the antarctic
13 boundary layer, *Atmos. Chem. Phys.*, 10, 10187-10209, 10.5194/acp-10-10187-2010, 2010.

14 Carslaw, N., Creasey, D. J., Heard, D. E., Lewis, A. C., McQuaid, J. B., Pilling, M. J., Monks, P. S., Bandy,
15 B. J., and Penkett, S. A.: Modeling OH, HO₂, and RO₂ radicals in the marine boundary layer - 1. Model
16 construction and comparison with field measurements, *J Geophys Res-Atmos*, 104, 30241-30255,
17 Doi 10.1029/1999jd900783, 1999a.

18 Carslaw, N., Jacobs, P. J., and Pilling, M. J.: Modeling OH, HO₂, and RO₂ radicals in the marine
19 boundary layer 2. Mechanism reduction and uncertainty analysis, *J Geophys Res-Atmos*, 104, 30257-
20 30273, Doi 10.1029/1999jd900782, 1999b.

21 Carslaw, N., Creasey, D. J., Harrison, D., Heard, D. E., Hunter, M. C., Jacobs, P. J., Jenkin, M. E., Lee, J.
22 D., Lewis, A. C., Pilling, M. J., Saunders, S. M., and Seakins, P. W.: OH and HO₂ radical chemistry in a
23 forested region of north-western Greece, *Atmos Environ*, 35, 4725-4737, Doi 10.1016/S1352-
24 2310(01)00089-9, 2001.

25 Carslaw, N., Creasey, D. J., Heard, D. E., Jacobs, P. J., Lee, J. D., Lewis, A. C., McQuaid, J. B., Pilling, M.
26 J., Bauguitte, S., Penkett, S. A., Monks, P. S., and Salisbury, G.: Eastern Atlantic Spring Experiment
27 1997 (EASE97) - 2. Comparisons of model concentrations of OH, HO₂, and RO₂ with measurements, *J*
28 *Geophys Res-Atmos*, 107, Doi 10.1029/2001jd001568, 2002.

29 Cleary, P. A., Romero, M. T. B., Blitz, M. A., Heard, D. E., Pilling, M. J., Seakins, P. W., and Wang, L.:
30 Determination of the temperature and pressure dependence of the reaction OH+C₂H₄ from 200-400
31 K using experimental and master equation analyses, *Phys Chem Chem Phys*, 8, 5633-5642, Doi
32 10.1039/B612127f, 2006.

33 Commane, R., Floquet, C. F. A., Ingham, T., Stone, D., Evans, M. J., and Heard, D. E.: Observations of
34 OH and HO₂ radicals over West Africa, *Atmos Chem Phys*, 10, 8783-8801, DOI 10.5194/acp-10-8783-
35 2010, 2010.

36 Creasey, D. J., HalfordMaw, P. A., Heard, D. E., Pilling, M. J., and Whitaker, B. J.: Implementation and
37 initial deployment of a field instrument for measurement of OH and HO₂ in the troposphere by laser-
38 induced fluorescence, *J Chem Soc Faraday T*, 93, 2907-2913, Doi 10.1039/A701469d, 1997a.

39 Creasey, D. J., Heard, D. E., Pilling, M. J., Whitaker, B. J., Berzins, M., and Fairlie, R.: Visualisation of a
40 supersonic free-jet expansion using laser-induced fluorescence spectroscopy: Application to the
41 measurement of rate constants at ultralow temperatures, *Appl Phys B-Lasers O*, 65, 375-391, DOI
42 10.1007/s003400050285, 1997b.

43 Creasey, D. J., Heard, D. E., and Lee, J. D.: OH and HO₂ measurements in a forested region of north-
44 western Greece, *Atmos Environ*, 35, 4713-4724, Doi 10.1016/S1352-2310(01)00090-5, 2001.

45 Creasey, D. J., Heard, D. E., and Lee, J. D.: Eastern Atlantic Spring Experiment 1997 (EASE97) 1.
46 Measurements of OH and HO₂ concentrations at Mace Head, Ireland, *J Geophys Res-Atmos*, 107,
47 Artn 4091 Doi 10.1029/2001jd000892, 2002.

48 Creasey, D. J., Evans, G. E., Heard, D. E., and Lee, J. D.: Measurements of OH and HO₂ concentrations
49 in the Southern Ocean marine boundary layer, *J Geophys Res-Atmos*, 108, Artn 4475 Doi
50 10.1029/2002jd003206, 2003.

1 Davis, D. D., Rodgers, M. O., Fischer, S. D., and Asai, K.: An experimental assessment of the O₃/H₂O
2 interference problem in the detection of natural levels of OH via laser induced fluorescence,
3 Geophysical Research Letters, 8, 69, 1981.

4 Emmerson, K. M., Carslaw, N., Carpenter, L. J., E., H. D., Lee, J. D., and Pilling, M. J.: Urban
5 Atmospheric Chemistry During the PUMA Campaign 1: Comparison of Modelled OH and HO₂
6 Concentrations with Measurements, Journal of Atmospheric Chemistry, 52, 143-164, 2005.

7 Emmerson, K. M., Carslaw, N., Carslaw, D. C., Lee, J. D., McFiggans, G., Bloss, W. J., Gravestock, T.,
8 Heard, D. E., Hopkins, J., Ingham, T., Pilling, M. J., Smith, S. C., Jacob, M., and Monks, P. S.: Free
9 radical modelling studies during the UK TORCH Campaign in Summer 2003, Atmospheric Chemistry
10 and Physics, 7, 167–181, 2007.

11 Faloon, I., Tan, D., Brune, W., Hurst, J., Barket, D., Couch, T. L., Shepson, P., Apel, E., Riemer, D.,
12 Thornberry, T., Carroll, M. A., Sillman, S., Keeler, G. J., Sagady, J., Hooper, D., and Paterson, K.:
13 Nighttime observations of anomalously high levels of hydroxyl radicals above a deciduous forest
14 canopy, J Geophys Res-Atmos, 106, 24315-24333, Doi 10.1029/2000jd900691, 2001.

15 Fuchs, H., Holland, F., and Hofzumahaus, A.: Measurement of tropospheric RO₂ and HO₂ radicals by a
16 laser-induced fluorescence instrument, Rev Sci Instrum, 79, Artn 084104 Doi 10.1063/1.29687121,
17 2008.

18 Fuchs, H., Bohn, B., Hofzumahaus, A., Holland, F., Lu, K. D., Nehr, S., Rohrer, F., and Wahner, A.:
19 Detection of HO₂ by laser-induced fluorescence: calibration and interferences from RO₂ radicals,
20 Atmos Meas Tech, 4, 1209-1225, DOI 10.5194/amt-4-1209-2011, 2011.

21 Fuchs, H., Dorn, H. P., Bachner, M., Bohn, B., Brauers, T., Gomm, S., Hofzumahaus, A., Holland, F.,
22 Nehr, S., Rohrer, F., Tillmann, R., and Wahner, A.: Comparison of OH concentration measurements
23 by DOAS and LIF during SAPHIR chamber experiments at high OH reactivity and low NO
24 concentration, Atmos Meas Tech, 5, 1611-1626, DOI 10.5194/amt-5-1611-2012, 2012.

25 Hanisco, T. F., Smith, J. B., Stimpfle, R. M., Wilmouth, D. M., Anderson, J. G., Richard, E. C., and Bui, T.
26 P.: In situ observations of HO₂ and OH obtained on the NASA ER-2 in the high-CIO conditions of the
27 1999/2000 Arctic polar vortex, J Geophys Res-Atmos, 107, Artn 8283 Doi 10.1029/2001jd001024,
28 2002.

29 Hard, T. M., O'Brien, R. J., Cook, T. B., and Tsongas, G. A.: Interference Suppression in OH
30 Fluorescence Detection, Appl Optics, 18, 3216-3217, Doi 10.1364/Ao.18.003216, 1979.

31 Hard, T. M., O'Brien, R. J., Chan, C. Y., and Mehrabzadeh, A. A.: Tropospheric Free-Radical
32 Determination by Fage, Environ Sci Technol, 18, 768-777, Doi 10.1021/Es00128a009, 1984.

33 Heard, D. E., and Pilling, M. J.: Measurement of OH and HO₂ in the troposphere, Chem Rev, 103,
34 5163-5198, Doi 10.1021/Cr020522s, 2003.

35 Heard, D. E., Carpenter, L. J., Creasey, D. J., Hopkins, J. R., Lee, J. D., Lewis, A. C., Pilling, M. J.,
36 Seakins, P. W., Carslaw, N., and Emmerson, K. M.: High levels of the hydroxyl radical in the winter
37 urban troposphere, Geophys Res Lett, 31, Artn L18112 Doi 10.1029/2004gl020544, 2004.

38 Heicklen, J.: The Decomposition of Alkyl Nitrites and the Reactions of Alkoxy Radicals, in: Advances
39 in Photochemistry, John Wiley & Sons, Inc., 177-272, 2007.

40 Hewitt, C. N., Lee, J. D., MacKenzie, A. R., Barkley, M. P., Carslaw, N., Carver, G. D., Chappell, N. A.,
41 Coe, H., Collier, C., Commane, R., Davies, F., Davison, B., Di Carlo, P., Di Marco, C. F., Dorsey, J. R.,
42 Edwards, P. M., Evans, M. J., Fowler, D., Furneaux, K. L., Gallagher, M., Guenther, A., Heard, D. E.,
43 Helfter, C., Hopkins, J., Ingham, T., Irwin, M., Jones, C., Karunaharan, A., Langford, B., Lewis, A. C.,
44 Lim, S. F., MacDonald, S. M., Mahajan, A. S., Malpass, S., McFiggans, G., Mills, G., Misztal, P., Moller,
45 S., Monks, P. S., Nemitz, E., Nicolas-Perea, V., Oetjen, H., Oram, D. E., Palmer, P. I., Phillips, G. J., Pike,
46 R., Plane, J. M. C., Pugh, T., Pyle, J. A., Reeves, C. E., Robinson, N. H., Stewart, D., Stone, D., Whalley,
47 L. K., and Yin, X.: Overview: oxidant and particle photochemical processes above a south-east Asian
48 tropical rainforest (the OP3 project): introduction, rationale, location characteristics and tools,
49 Atmos Chem Phys, 10, 169-199, DOI 10.5194/acp-10-169-2010, 2010.

1 Hofzumahaus, A., Aschmutat, U., Hessling, M., Holland, F., and Ehhalt, D. H.: The measurement of
2 tropospheric OH radicals by laser-induced fluorescence spectroscopy during the POPCORN field
3 campaign, *Geophys Res Lett*, 23, 2541-2544, Doi 10.1029/96gl02205, 1996.

4 Holland, F., Hofzumahaus, A., Schafer, R., Kraus, A., and Patz, H. W.: Measurements of OH and HO₂
5 radical concentrations and photolysis frequencies during BERLIOZ, *J Geophys Res-Atmos*, 108, Art
6 8246 Doi 10.1029/2001jd001393, 2003.

7 Ianni, J. C.: www.kintecus.com, in, Windows version 2.80 ed., 2002.

8 Jenkin, M. E., Saunders, S. M., and Pilling, M. J.: The tropospheric degradation of volatile organic
9 compounds: A protocol for mechanism development, *Atmos Environ*, 31, 81-104, Doi
10 10.1016/S1352-2310(96)00105-7, 1997.

11 Jenkin, M. E., Saunders, S. M., Wagner, V., and Pilling, M. J.: Protocol for the development of the
12 Master Chemical Mechanism, MCM v3 (Part B): tropospheric degradation of aromatic volatile
13 organic compounds, *Atmos Chem Phys*, 3, 181-193, 2003.

14 Kanaya, Y., Sadanaga, Y., Matsumoto, J., Sharma, U. K., Hirokawa, J., Kajii, Y., and Akimoto, H.:
15 Nighttime observation of the HO₂ radical by an LIF instrument at Oki island, Japan, and its possible
16 origins, *Geophys Res Lett*, 26, 2179-2182, Doi 10.1029/1999gl900475, 1999.

17 Kukui, A., and Le Bras, G.: Theoretical study of the thermal decomposition of several beta-
18 chloroalkoxy radicals, *Phys Chem Chem Phys*, 3, 175-178, Doi 10.1039/B007644i, 2001.

19 Lu, K. D., Rohrer, F., Holland, F., Fuchs, H., Bohn, B., Brauers, T., Chang, C. C., Haseler, R., Hu, M., Kita,
20 K., Kondo, Y., Li, X., Lou, S. R., Nehr, S., Shao, M., Zeng, L. M., Wahner, A., Zhang, Y. H., and
21 Hofzumahaus, A.: Observation and modelling of OH and HO₂ concentrations in the Pearl River Delta
22 2006: a missing OH source in a VOC rich atmosphere, *Atmos Chem Phys*, 12, 1541-1569, DOI
23 10.5194/acp-12-1541-2012, 2012.

24 Mao, J., Ren, X., Zhang, L., Van Duin, D. M., Cohen, R. C., Park, J. H., Goldstein, A. H., Paulot, F.,
25 Beaver, M. R., Crouse, J. D., Wennberg, P. O., DiGangi, J. P., Henry, S. B., Keutsch, F. N., Park, C.,
26 Schade, G. W., Wolfe, G. M., Thornton, J. A., and Brune, W. H.: Insights into hydroxyl measurements
27 and atmospheric oxidation in a California forest, *Atmos Chem Phys*, 12, 8009-8020, DOI
28 10.5194/acp-12-8009-2012, 2012.

29 Mather, J. H., Stevens, P. S., and Brune, W. H.: OH and HO₂ measurements using laser-induced
30 fluorescence, *J Geophys Res-Atmos*, 102, 6427-6436, Doi 10.1029/96jd01702, 1997.

31 Nehr, S., Bohn, B., and Wahner, A.: Prompt HO₂ Formation Following the Reaction of OH with
32 Aromatic Compounds under Atmospheric Conditions, *J Phys Chem A*, 116, 6015-6026, Doi
33 10.1021/Jp210946y, 2012.

34 Orlando, J. J., Tyndall, G. S., and Wallington, T. J.: The atmospheric chemistry of alkoxy radicals,
35 *Chem Rev*, 103, 4657-4689, Doi 10.1021/Cr020527p, 2003.

36 Ortgies, G., Gericke, K. H., and Comes, F. J.: Is UV Laser-Induced Fluorescence a method to monitor
37 tropospheric OH?, *Geophys Res Lett*, 7, 905-908, Doi 10.1029/Gl007i011p00905, 1980.

38 Peeters, J., Nguyen, T. L., and Vereecken, L.: HO_x radical regeneration in the oxidation of isoprene,
39 *Physical Chemistry and Chemical Physics*, 11, 5935-5939, 2009.

40 Ren, X. R., Harder, H., Martinez, M., Faloona, I. C., Tan, D., Leshner, R. L., Di Carlo, P., Simpas, J. B., and
41 Brune, W. H.: Interference testing for atmospheric HO_x measurements by laser-induced
42 fluorescence, *J Atmos Chem*, 47, 169-190, Doi 10.1023/B:Joch.0000021037.46866.81, 2004.

43 Sadanaga, Y., Yoshino, A., Watanabe, K., Yoshioka, A., Wakazono, Y., Kanaya, Y., and Kajii, Y.:
44 Development of a measurement system of OH reactivity in the atmosphere using a laser-induced
45 pupm and probe technique, *Review of Scientific Instruments*, 75, 2648-2655, 2004.

46 Saunders, S. M., Jenkin, M. E., Derwent, R. G., and Pilling, M. J.: Protocol for the development of the
47 Master Chemical Mechanism, MCM v3 (Part A): tropospheric degradation of non-aromatic volatile
48 organic compounds, *Atmos Chem Phys*, 3, 161-180, 2003.

49 Shirinzadeh, B., Wang, C. C., and Deng, D. Q.: new copy required, *Applied Optics*, 26, 2102, 1987.

1 Smith, S. C., Lee, J. D., Bloss, W. J., Johnson, G. P., Ingham, T., and Heard, D. E.: Concentrations of OH
2 and HO₂ radicals during NAMBLEX: measurements and steady state analysis, *Atmos Chem Phys*, 6,
3 1435-1453, 2006.

4 Sommariva, R., Haggerstone, A. L., Carpenter, L. J., Carslaw, N., Creasey, D. J., Heard, D. E., Lee, J. D.,
5 Lewis, A. C., Pilling, M. J., and Zador, J.: OH and HO₂ chemistry in clean marine air during SOAPEX-2,
6 *Atmos Chem Phys*, 4, 839-856, 2004.

7 Sommariva, R., Bloss, W. J., Brough, N., Carslaw, N., Flynn, M., Haggerstone, A. L., Heard, D. E.,
8 Hopkins, J. R., Lee, J. D., Lewis, A. C., McFiggans, G., Monks, P. S., Penkett, S. A., Pilling, M. J., Plane, J.
9 M. C., Read, K. A., Saiz-Lopez, A., Rickard, A. R., and Williams, P. I.: OH and HO₂ chemistry during
10 NAMBLEX: roles of oxygenates, halogen oxides and heterogeneous uptake, *Atmos Chem Phys*, 6,
11 1135-1153, 2006.

12 Stevens, P. S., Mather, J. H., and Brune, W. H.: Measurement of Tropospheric OH and HO₂ by Laser-
13 Induced Fluorescence at Low-Pressure, *J Geophys Res-Atmos*, 99, 3543-3557, Doi
14 10.1029/93jd03342, 1994.

15 Stone, D., Whalley, L. K., and Heard, D. E.: Tropospheric OH and HO₂ radicals: field measurements
16 and model comparisons, *Chem Soc Rev*, 41, 6348-6404, Doi 10.1039/C2cs35140d, 2012.

17 Vaughan, S., Ingham, T., Whalley, L. K., Stone, D., Evans, M. J., Read, K. A., Lee, J. D., Moller, S. J.,
18 Carpenter, L. J., Lewis, A. C., Fleming, Z. L., and Heard, D. E.: Seasonal observations of OH and HO₂ in
19 the remote tropical marine boundary layer, *Atmos Chem Phys*, 12, 2149-2172, DOI 10.5194/acp-12-
20 2149-2012, 2012.

21 Whalley, L. K., Furneaux, K. L., Goddard, A., Lee, J. D., Mahajan, A., Oetjen, H., Read, K. A., Kaaden,
22 N., Carpenter, L. J., Lewis, A. C., Plane, J. M. C., Saltzman, E. S., Wiedensohler, A., and Heard, D. E.:
23 The chemistry of OH and HO₂ radicals in the boundary layer over the tropical Atlantic Ocean, *Atmos*
24 *Chem Phys*, 10, 1555-1576, DOI 10.5194/acp-10-1555-2010, 2010.

25 Whalley, L. K., Edwards, P. M., Furneaux, K. L., Goddard, A., Ingham, T., Evans, M. J., Stone, D.,
26 Hopkins, J. R., Jones, C. E., Karunaharan, A., Lee, J. D., Lewis, A. C., Monks, P. S., Moller, S. J., and
27 Heard, D. E.: Quantifying the magnitude of a missing hydroxyl radical source in a tropical rainforest,
28 *Atmos Chem Phys*, 11, 7223-7233, DOI 10.5194/acp-11-7223-2011, 2011.

29 Whalley, L. K., Stone, D., George, I., Mertes, S., Van Pinxteren, D., Fomba, K. W., Herrmann, H., and
30 Heard, D. E.: The influence of clouds on radical concentrations: Observations of OH and HO₂ during
31 the Hill Cap Cloud Thuringer (HCCT) campaign in 2010, *Geophys Res Lett*, To be submitted, 2013.

32

33

- 1 Table 1: Experimentally determined OH yields (derived using Eq. 1) from peroxy radicals ($\text{RO}_2 \rightarrow \text{HO}_2 \rightarrow \text{OH}$) in continuous flow experiments
- 2 for FAGE cells operated under fieldwork conditions and comparison with the MCMv3.2 OH yield. The modelled OH yield was determined
- 3 using Eq. 4.

Source of peroxy radicals	Flow of NO (SCCM)	Cell A, OH yield Residence time: $\sim 0.9 \text{ ms}^1$ Typical NO flow used during fieldwork: 50 SCCM ² Flow rate through pinhole: 4.8 SLM Cell Pressure: 0.9 Torr	MCM OH yield (referenced to initial $[\text{RO}_2]$) assuming a reaction time of 0.9 ms, a temperature of 255K and $[\text{NO}] = 1 \times 10^{14} \text{ molecule cm}^{-3}$	Cell B, OH yield Residence time: $\sim 1.9 \text{ ms}^3$ Typical NO flow used during fieldwork: 10 SCCM Flow rate through pinhole: 3 SLM Cell Pressure: 1 Torr	MCM OH yield (referenced to initial $[\text{RO}_2]$) assuming a reaction time of 1.9 ms, a temperature of 255K and $[\text{NO}] = 1 \times 10^{14} \text{ molecule cm}^{-3}$	Cell C, OH yield Residence time: $\sim 60 \text{ ms}^3$ Typical NO flow used during fieldwork: 100 SCCM Flow rate through pinhole: 3.5 SLM Cell Pressure: 1.5 Torr	MCM OH yield (referenced to initial $[\text{RO}_2]$) assuming a reaction time of 70 ms, a temperature of 298K and $[\text{NO}] = 9.5 \times 10^{14} \text{ molecule cm}^{-3}$
Ethene	10	0.057 \pm 0.033		0.463 \pm 0.030	0.446	-	
	20	0.073 \pm 0.029		-		-	
	30	0.098 \pm 0.025		-		-	
	40	0.157 \pm 0.047		-		-	

	50	0.172±0.057	0.170	-		-	
	100	-		-		0.947±0.073	0.936
Methanol	50	0.756±0.273	1.000	-		-	
Isoprene	50	0.178±0.075	0.175	-		0.849±0.057	0.871
Propane	50	0.000±0.053	0.004	0.000±0.102	0.004	-	
Methane	100	-		-		0.000±0.091	4.8×10 ⁻⁴
Cyclohexane	100	-		-		0.606±0.051	0.575
Toluene	100	-		-		0.874±0.072	0.900

- 1 ¹ determined by computational fluid dynamics, for further details refer to Creasey et al. (1997b)
- 2 ² experiments during which the NO concentration was varied from 10 – 50 SCCM and compared to modelled OH yields (see Fig. 4) suggest that
- 3 NO that mixes into to the air flow is actually 5.5 times less than the NO that is injected.
- 4 ³ estimated from comparison of experimentally determined OH yield from ethane-derived RO₂ radicals and MCM-predicted yields.

1 Table 2: OH yields in time-resolved experiments from peroxy radicals determined using Eq.
 2 2 and Eq. 3; the MCMv3.2 OH yield is provided in the final columns for comparison. The
 3 modelled OH yield was determined using Eq. 4 calculated after 9.8 ms integration time. The
 4 model was constrained with a $[\text{NO}] = 1 \times 10^{14}$ molecule cm^{-3} and a temperature = 298 K
 5 (fourth column) or $[\text{NO}] = 1 \times 10^{14}$ molecule cm^{-3} and a temperature = 255 K (final column).

Source of peroxy radicals	OH yield (referenced to methanol)	OH Yield (referenced to ethene)	MCM OH yield (referenced to initial $[\text{RO}_2]$) at 298 K	MCM OH yield (referenced to initial $[\text{RO}_2]$) at 255 K
Methanol	1.00 ± 0.08	0.85 ± 0.09	1.00	-
Isoprene	0.89 ± 0.05	0.92 ± 0.04	0.90	-
Ethene	1.06 ± 0.04	1.00 ± 0.08	0.99	0.90
Cyclohexane		0.38 ± 0.08	0.74	0.36
Propane		0.034 ± 0.008	0.01	-
n-Butane		0.18 ± 0.01	0.13	0.12
n-Pentane		0.48 ± 0.01	0.62	0.49

6

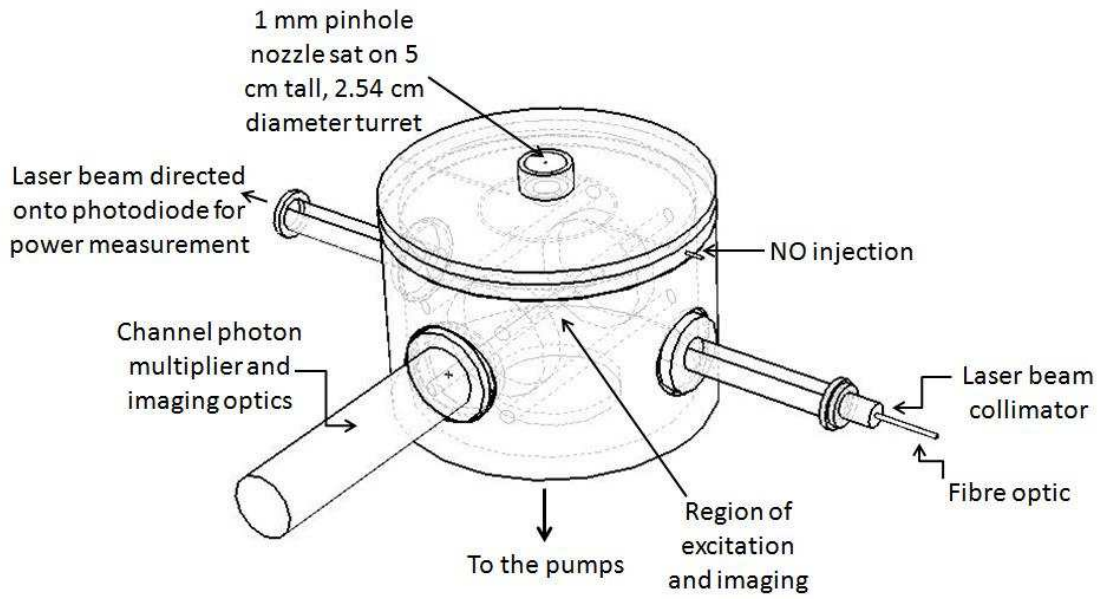
7

- 1 Table 3: Model : measured HO₂ ratio reported for the University of Leeds ground-based
- 2 FAGE system during field campaigns where HO₂ measurements were made.

Campaign	Model-measurement agreement for HO ₂	Cell-type	Reference
EASE-96	Limited data, but tendency for model to overestimate HO ₂	A	(Carslaw et al., 1999a)
AEROBIC	Modelled HO ₂ was typically higher than observations, but observations showed a high degree of variability	A	(Carslaw et al., 2001)
EASE-97	Modelled:measured ratio of 3.6	A	(Carslaw et al., 2002)
SOAPEX	Modelled : measured ratio of 1.4	A	(Sommariva et al., 2004)
PUMA-summer	modelled : measured ratio of 0.56	A	(Emmerson et al., 2005)
PUMA-winter	modelled : measured ratio of 0.49	A	(Emmerson et al., 2005)
NAMBLEX	Good agreement within combined uncertainties	A	(Sommariva et al., 2006)
TORCH	Good agreement within combined uncertainties; modelled : measured ratio of 1.07	A	(Emmerson et al., 2007)
CHABLIS	Model : measured ratio of 2	A	(Bloss et al., 2010)
RHaMBLe	Good agreement within combined uncertainties	A	(Whalley et al., 2010)
OP3	modelled : measured ratio of 1.75 (standard chemistry model)	A	(Whalley et al., 2011)
HCCT	Good agreement within combined uncertainties during the daytime	B	(Whalley et al., 2013)
ClearLo	modelling studies underway	A & C	

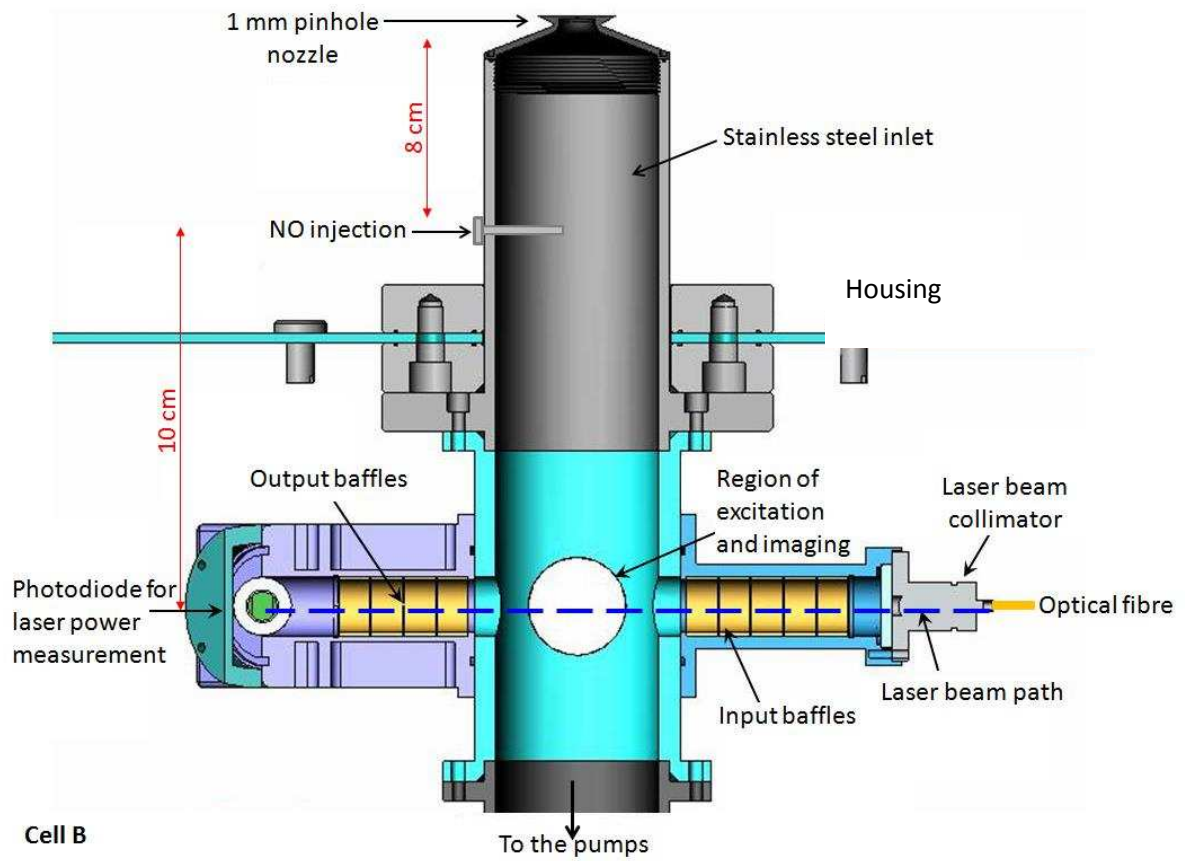
3

4



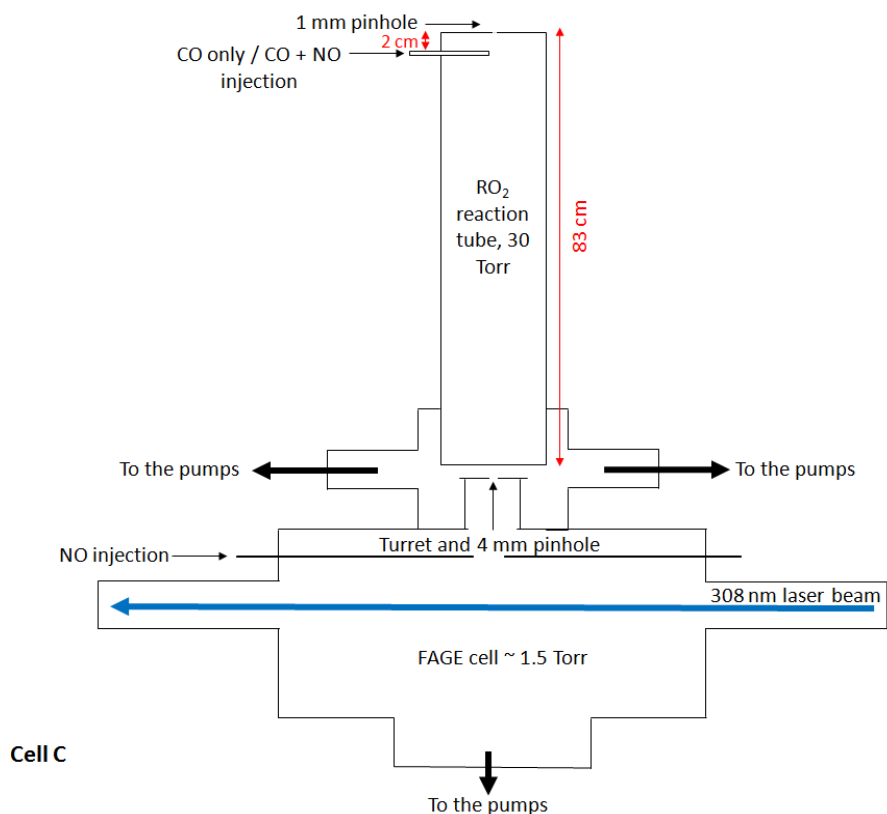
Cell A

1



Cell B

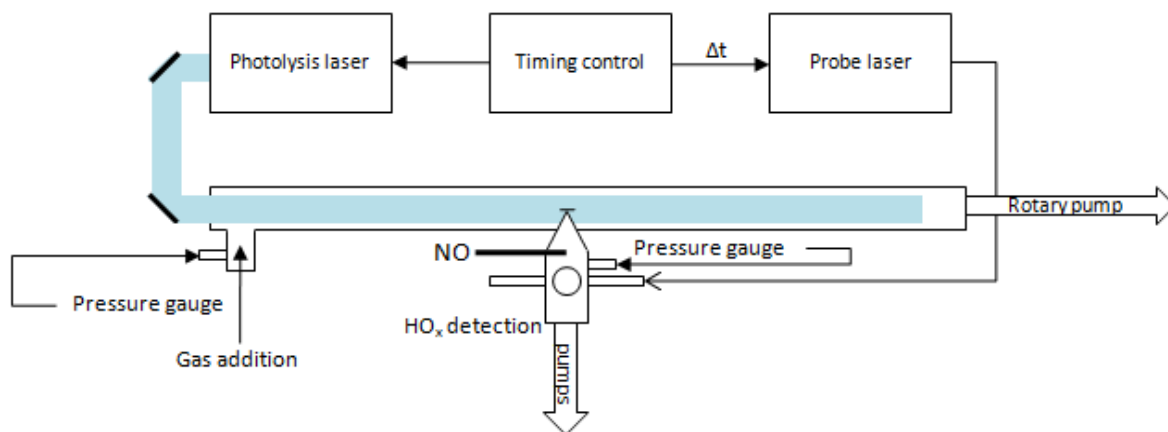
2



1

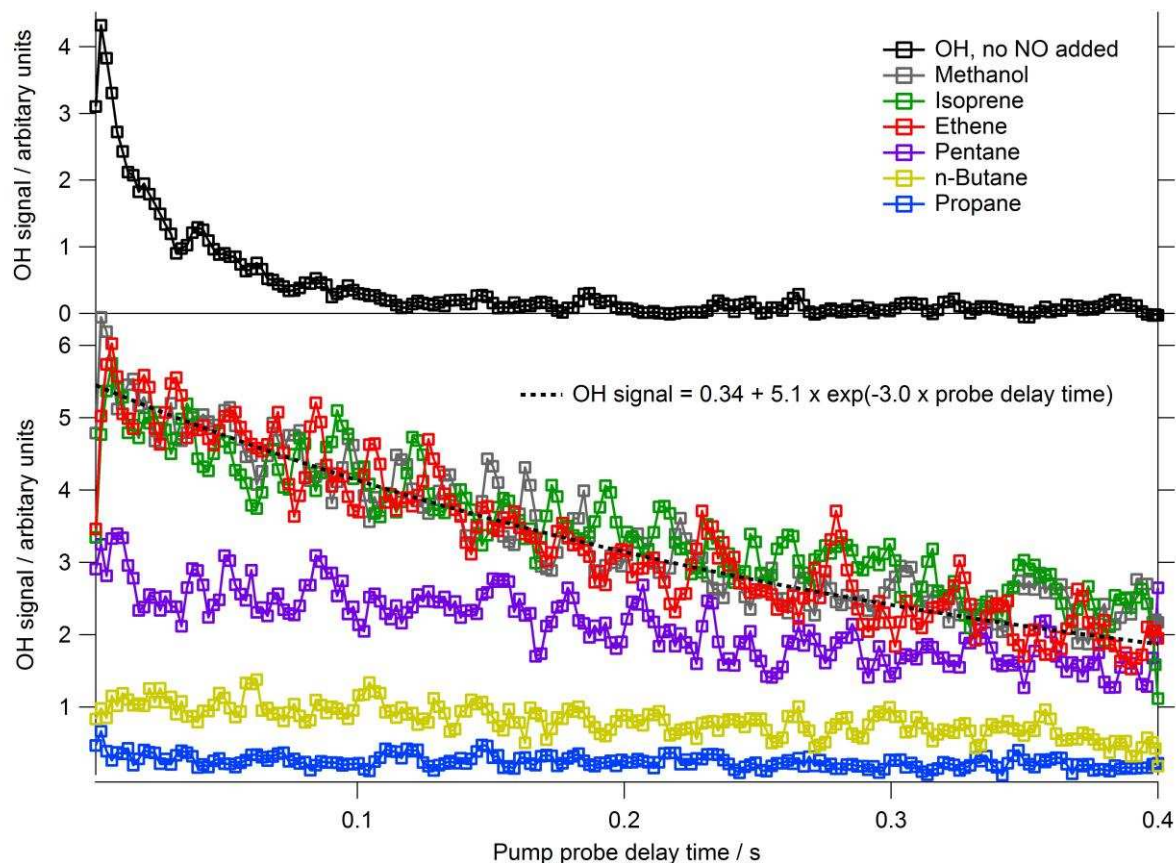
2 Figure 1: Schematics highlighting the key features of the three FAGE cells tested. Cell A was
 3 used for sequential OH and HO₂ detection during the OP3 project; dotted line highlights
 4 internal cell components. Cell B was used to make sequential tower-based measurements of
 5 OH and HO₂ during the HCCT campaign. Cell C represents the coupling of a reaction tube to
 6 a FAGE cell (cell A design) for detection of RO₂ radicals by LIF, see text for further details.

7

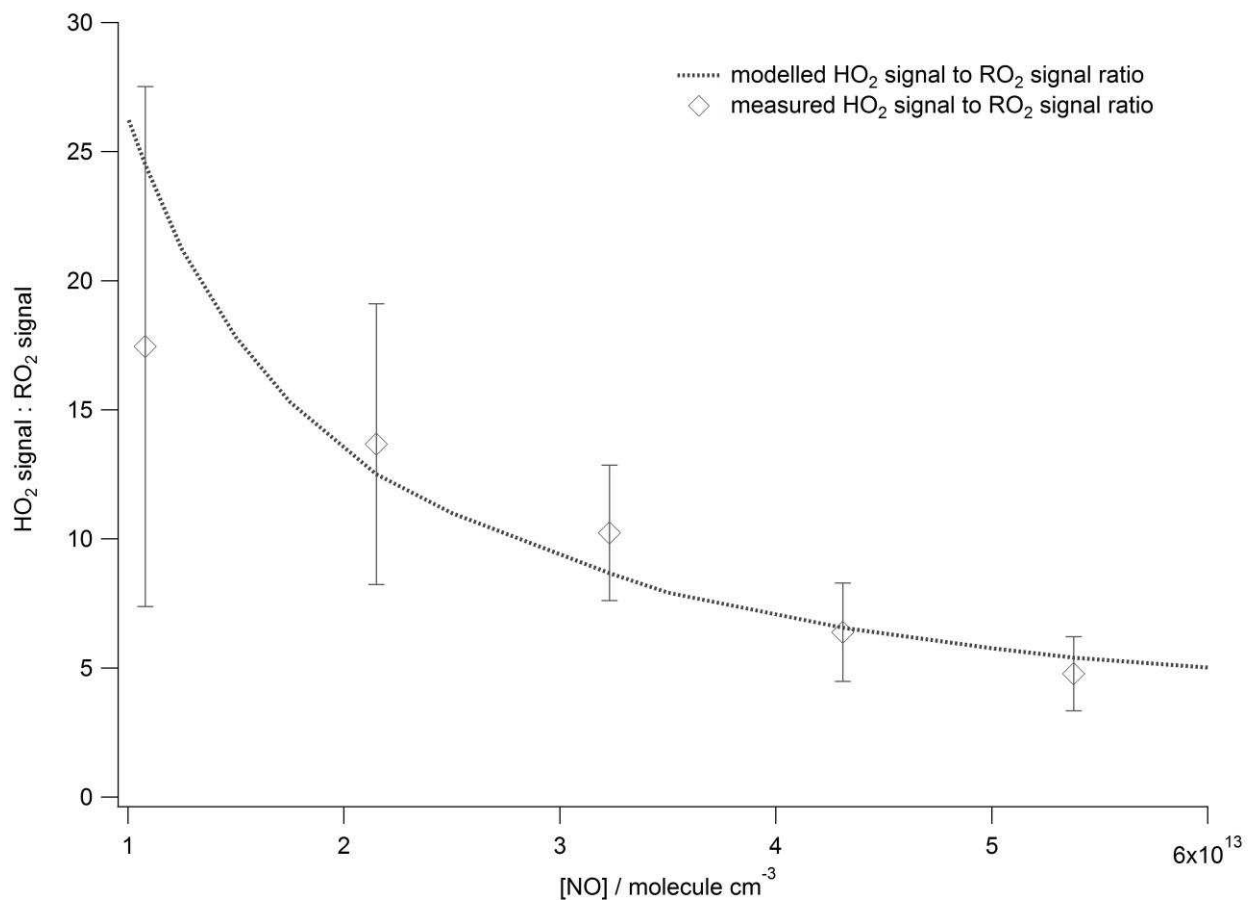


8

9 Figure 2: Schematic highlighting the key features of the laser flash-photolysis time-resolved
 10 experimental set-up.



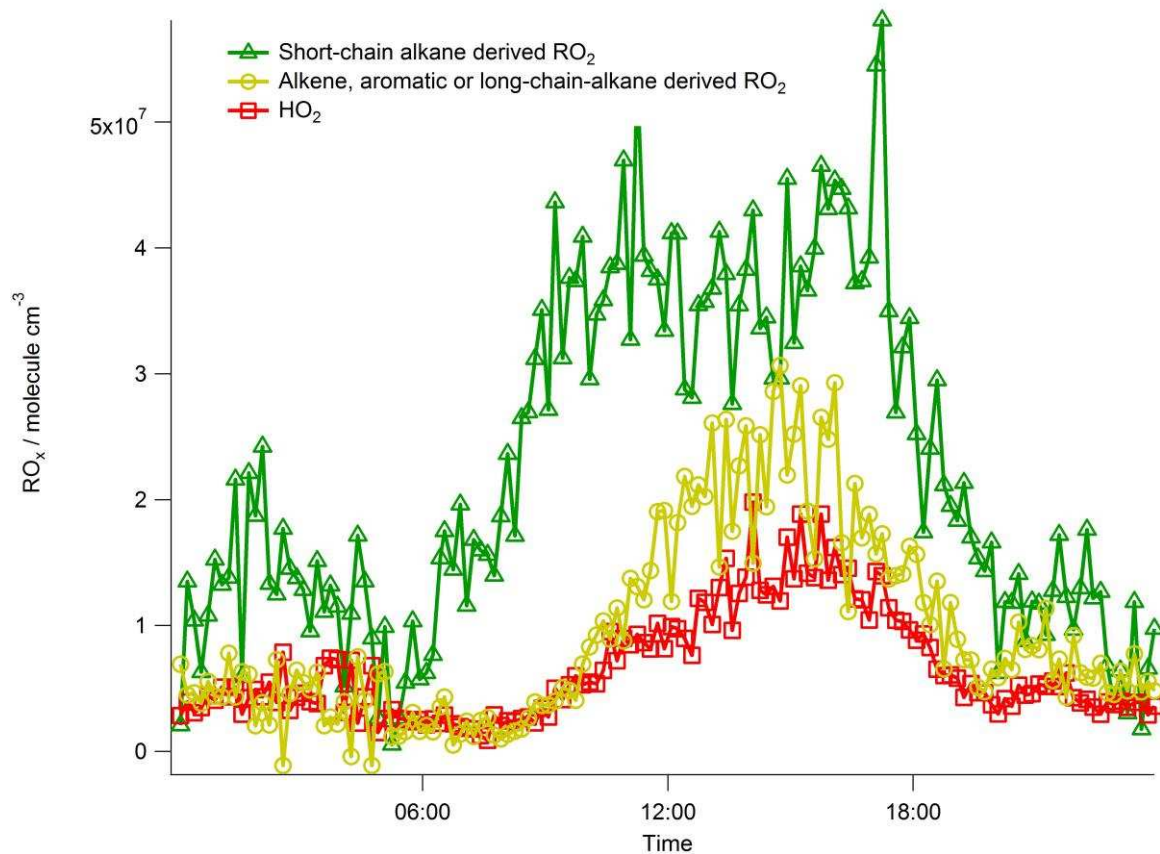
1
 2 Figure 3, upper panel: Time evolution of OH formed in the flow tube by laser-photolysis of
 3 O_3 in humidified air in the absence of reagent with no NO added to the FAGE cell. The
 4 observed decay of $\sim 25 \text{ s}^{-1}$ may be attributed to reaction of OH with ozone and diffusion of
 5 the radical out of the photolysis beam area. Lower panel: Typical time-resolved experiments
 6 showing the OH signal from isoprene (green), ethene (red), methanol (grey), n-pentane
 7 (purple), n-butane (mustard) and propane (blue) derived peroxy radicals that was observed
 8 when 6 SCCM NO was added to the FAGE cell, and the relevant VOC reagent added to the
 9 flow tube to convert OH quantitatively to RO_2 . The dashed line shows the fit to the OH signal
 10 from ethene-derived RO_2 radicals of the function:
 11 $OH \text{ signal} = y_0 + A \times \exp(-B \times \text{probedelay time})$. The signal decay ($\sim 5 \text{ s}^{-1}$) observed in the
 12 lower panel may be attributed primarily to diffusion of the radicals out of the photolysis beam
 13 area and to a lesser extent ($\sim 1 \text{ s}^{-1}$) to radical-radical reaction. The relative yields were
 14 determined from the ratio of the A factors. See Table 2 for the yields determined.



1

2 Figure 4: Modelled (dashed line) and measured (open diamonds) ratio of the OH yield from
 3 HO₂ signal: RO₂ signal as a function of NO concentration determined for cell A. For best
 4 agreement with model predictions, it has to be assumed that the NO concentration that mixes
 5 into the ambient air stream is 5.5 times lower than the amount actually injected. The error
 6 bars represent the fractional error associated with each measured ratio determined from the
 7 1σ standard deviation of the experiments conducted.

8



1

2 Figure 5: Campaign averaged diurnal profiles of short-chain alkane RO₂ radicals (green),
 3 HO₂ (red) and alkene or aromatic or long-chain-alkane derived RO₂ radicals (mustard) from
 4 the ClearfLo project which took place in London (North Kensington) from the 21st July to
 5 18th August 2012.